

THERMODYNAMICALLY CONSISTENT DYNAMIC BOUNDARY CONDITIONS OF PHASE FIELD MODELS*

XIAOBO JING[†] AND QI WANG[‡]

Abstract. We present a general, constructive method to derive thermodynamically consistent models and consistent dynamic boundary conditions hierarchically following the generalized Onsager principle. The method consists of two steps in tandem: the dynamical equation is determined by the generalized Onsager principle in the bulk firstly, and then the surface chemical potential and the thermodynamically consistent boundary conditions are formulated subsequently by applying the generalized Onsager principle at the boundary. The application strategy of the generalized Onsager principle in two-step yields thermodynamically consistent models together with the consistent boundary conditions that warrant a non-negative entropy production rate (or equivalently non-positive energy dissipation rate in isothermal cases) in the bulk as well as at the boundary. We illustrate the method using phase field models of binary materials elaborate on two sets of thermodynamically consistent dynamic boundary conditions. These two types of boundary conditions differ in how the across boundary mass flux participates in boundary surface dynamics. We then show that many existing thermodynamically consistent, binary phase field models together with their dynamic or static boundary conditions are derivable from this method. As an illustration, we show numerically how dynamic boundary conditions affect crystal growth in the bulk using a binary phase field model.

Keywords. Thermodynamically consistent model ;phase field model; dynamic boundary conditions; binary materials; energy dissipation.

AMS subject classifications. 35G30; 35G60; 35Q79; 35Q82

1. Introduction

Thermodynamically consistent models refer to the models that are derived from thermodynamical laws and principles. In particular, they obey the second law of thermodynamics, i.e., the entropy production rate is non-negative or equivalently the energy dissipation rate is non-positive in isothermal cases. The generalized Onsager principle is a protocol in which the Onsager linear response theory combined with the equilibrium maximum entropy principle is used to derive thermodynamically consistent models [44, 45, 56, 61]. The generalized Onsager principle warrants the second law of thermodynamics in the form of Clausius-Duhem inequality and has proven to be an effective modeling tool for developing thermodynamical models at various time and length scales [39, 55, 61, 64, 65]. In the past, the Onsager principle and the equivalent thermodynamical second law has been primarily used to derive dynamic equations in the bulk while boundary effects are largely ignored by assuming adiabatic and static boundary conditions or periodic boundary conditions. In this study, we present a general, hierarchical method to derive thermodynamically consistent models with consistent dynamic boundary conditions for material systems using the generalized Onsager principle in not only the bulk but also the boundaries, where the dynamic boundary conditions reduce to static ones in the limit. We illustrate the idea by deriving thermodynamically consistent phase field models and consistent boundary conditions for binary materials in a piecewise smooth domain owing to their abundance in the literature.

Phase field modeling has emerged as one of the powerful and versatile modeling paradigm in dealing with multiphase materials in domains with complex interface geometries and complex interfacial phenomena between distinct immiscible phases [52, 54, 59]. It is especially useful and effective when handling dynamic phase boundaries in multiphase materials involving topological changes compared to other methods such as front tracking methods, level-set

*Received date: April 12, 2022 and accepted date (in revised version): August 15, 2022.

[†]Beijing Computational Science Research Center, Beijing 100193, P. R. China and Department of Mathematics, University of South Carolina, Columbia, SC 29028, USA, (jingxb@csrc.ac.cn).

[‡]Department of Mathematics, University of South Carolina, Columbia, SC 29028, USA, (qwang@math.sc.edu).

methods, and volume of fluid methods etc [6, 52, 53]. By design, it is for diffuse interfaces with certain interface thickness in which complex interfacial dynamics prevails. A quality phase field model should be able to capture well-known sharp interface conditions (e.g Gibbs-Thomson condition) in the vanishing thickness of the interface [22, 51]. This requires one to be mindful when deriving the free energy of the system in the phase field model so that thermodynamical laws and principles are followed faithfully and properly. Notice that the advantage of the phase field model in dealing with diffuse interfaces may also limit its applicability to resolve sharp interfaces [13]. In life science, materials science and engineering, there are multiphase material systems with diffuse interfaces, which have kept multiphase field models popular and practical [33, 42, 47, 53].

There are quite a number of phase field models in the literature today. However, not all are thermodynamically consistent. In this study, we focus on the derivation of thermodynamically consistent phase field models, which include the derivation of the transport equation in the bulk as well as the consistent dynamic boundary conditions in fixed boundaries. We stress that it is important to study multiphase material systems using a thermodynamically "correct" model that not only gives one a comprehensive description of the correct physics, but also gives one a well-posed mathematical system to analyze and compute. Speaking of a thermodynamically "correct" model, we insist that the model must be at least thermodynamically consistent. This humble criterion would perhaps disqualify a host of existing phase field models. In addition, we notice that most of the studies on phase field models are concentrated on equations in the bulk with static or periodic boundary conditions at fixed boundaries, where the boundary contributions to thermodynamical consistency are trivialized.

Given the recent technological advances in materials science and engineering, boundaries of a material confining device can no longer be treated as passive. They can be made with distinctive properties to interact or even control the material within the device [24, 49, 62]. For instance, the newly discovered boundary effect to the existence of blue phases in cholesteric liquid crystals in microscales across a quite large temperature range is one of the prominent examples [5, 41, 48]. This requires one to derive a model for the material system to take into account the potential dynamic contribution from the boundary. There have been a surge in activities of this direction on phase field models recently [8, 9, 16, 17, 20, 23, 43]. Here, we briefly review some existing thermodynamically consistent phase field models with various static and dynamic boundary conditions.

When one studies dynamics of a phase field model in a fixed domain with adiabatic boundary conditions, no-flux boundary conditions are normally adopted as sufficient adiabatic conditions which contribute to a zero energy flux across the boundary. The most commonly studied phase field models are the Allen-Cahn and the Cahn-Hilliard model, respectively [1, 3]. We consider a binary material system in a domain Ω with the free energy given by

$$E = \int_{\Omega} \left[\frac{\epsilon}{2} |\nabla \phi|^2 + \frac{1}{\epsilon} f(\phi) \right] d\mathbf{x}, \quad (1.1)$$

where ϕ is a mass or volume fraction of one material's component, boundary $\partial\Omega$ is piecewise smooth, ϵ is the strength of the conformational entropy and $\frac{1}{\epsilon} f(\phi)$ is the bulk free energy density. For simplicity, we refer to ϕ as the mass fraction throughout the paper.

The Allen-Cahn equation [1] for dynamics of ϕ is given by

$$\phi_t = -M_b^{(1)} \mu, \quad \mu = \frac{\delta E}{\delta \phi}, \quad (1.2)$$

where $M_b^{(1)}$ is the positive semi-definite mobility operator and μ is known as the chemical potential. For adiabatic boundaries, one uses the following homogeneous Neumann boundary

condition (HNBC) to ensure that the energy dissipation of the system is dictated exclusively by bulk energy dissipation

$$\mathbf{n} \cdot \nabla \phi = \nabla_{\mathbf{n}} \phi = 0. \quad (1.3)$$

The energy dissipation rate in the model is given by the bulk integral without any boundary contributions

$$\frac{d}{dt} E = - \int_{\Omega} \mu M_b^{(1)} \mu d\mathbf{x}. \quad (1.4)$$

Notice that this model doesn't conserve mass. To conserve mass, one uses another one known as the Cahn-Hilliard model with homogeneous Neumann boundary condition (HNBC-CH model).

The Cahn-Hilliard equation [3] for dynamics of ϕ is given by

$$\phi_t = \nabla \cdot \mathbf{M}_b^{(2)} \cdot \nabla \mu, \quad \mu = \frac{\delta E}{\delta \phi}, \quad (1.5)$$

where $\mathbf{M}_b^{(2)}$ is the positive semi-definite mobility coefficient matrix. The following homogeneous Neumann boundary conditions ensure the mass conservation and energy dissipation for the model simultaneously

$$\mathbf{n} \cdot \mathbf{M}_b^{(2)} \cdot \nabla \mu = 0, \quad \mathbf{n} \cdot \nabla \phi = 0, \quad (1.6)$$

where the first equation is called the no mass flux condition, resulted from the variation in the energy dissipation rate, and the second condition ensures that no boundary energy fluxes result from the conformational entropy. Note that all these are static boundary conditions so that there is no boundary dynamics in this model. This is by far the most widely studied phase field model in the literature [7, 28, 50]. Besides the Cahn-Hilliard model, non-local constraints can be added to the Allen-Cahn model to enforce the mass conservation to yield the Allen-Cahn model with nonlocal constraints [28, 29].

If there are material and/or energy exchange across the boundary or there exists dynamics on the boundary, dynamics of materials in the bulk can be affected. Next, we list several binary phase field models with dynamic boundary conditions studied recently. The free energy of the binary material system of these models consists of two parts: the bulk free energy E_b and the surface free energy E_s , respectively,

$$E = E_b + E_s, \quad E_b = \int_{\Omega} \frac{\epsilon}{2} |\nabla \phi|^2 + \frac{1}{\epsilon} f(\phi) d\mathbf{x}, \quad E_s = \int_{\partial\Omega} \frac{\delta}{2} |\nabla_s \phi|^2 + \frac{1}{\delta} g(\phi) ds, \quad (1.7)$$

where $\nabla_s = \nabla - (\mathbf{n} \cdot \nabla) \mathbf{n} = (\mathbf{I} - \mathbf{n}\mathbf{n}) \nabla$ is the surface gradient operator [2, 10], δ is the strength of the conformational entropy at the boundary and $g(\phi)$ is the surface energy density at the boundary [14, 15, 32].

Gal et al derived a set of dynamic boundary conditions for the Cahn-Hilliard model in [18] (Gal model),

$$\begin{aligned} \frac{\partial \phi}{\partial t} &= M_b^{(2)} \Delta \mu, \quad \mu = -\epsilon \Delta \phi + \frac{1}{\epsilon} f'(\phi), \quad \mathbf{x} \in \Omega, \\ \frac{\partial \phi}{\partial t} &= -\mu_s - \beta M_b^{(2)} \nabla_{\mathbf{n}} \mu, \quad \mathbf{x} \in \partial\Omega, \\ \mu_s &= -\delta \Delta_s \phi + \frac{1}{\delta} g'(\phi) + \epsilon \nabla_{\mathbf{n}} \phi, \quad \mu = \beta \mu_s, \quad \mathbf{x} \in \partial\Omega, \\ \phi(\mathbf{x}, 0) &= \phi_0(\mathbf{x}), \quad \mathbf{x} \in \Omega \cup \partial\Omega, \end{aligned} \quad (1.8)$$

where $\nabla_{\mathbf{n}} = \mathbf{n} \cdot \nabla$, and Δ_s is the Laplace-Beltrami operator [10, 27]. In this model, the mobility operator is given by $M_b^{(2)} \Delta$ with a constant mobility coefficient $M_b^{(2)}$ and the energy dissipation rate is given by

$$\frac{d}{dt} E = -M_b^{(2)} \int_{\Omega} |\nabla \mu|^2 d\mathbf{x} - \int_{\partial\Omega} |\mu_s|^2 ds. \quad (1.9)$$

At the boundary, the chemical potential from the bulk is stipulated to be proportional to the chemical potential at the surface with proportionality parameter β ; the effective chemical potential at the surface includes a flux contribution from the bulk; the dynamic equation of the mass fraction on the surface follows Allen-Cahn dynamics with an additional flux from the bulk so that it does not conserve any quantities as seen in other models below. Neither mass of the bulk nor mass of the boundary is conserved in this model. If we choose $g = \delta = 0$ and let $\beta \rightarrow \infty$, the Gal model reduces to the HNBC-CH model.

In 2011, Goldstein et al [26] modified the boundary transport equation of the mass fraction in the Cahn-Hilliard model to give the following governing system of equations (GMS model)

$$\begin{aligned} \frac{\partial \phi}{\partial t} &= M_b^{(2)} \Delta \mu, \quad \mu = -\epsilon \Delta \phi + \frac{1}{\epsilon} f'(\phi), \quad \mathbf{x} \in \Omega, \\ \frac{\partial \phi}{\partial t} &= M_s^{(2)} \Delta_s \mu_s - \beta M_b^{(2)} \nabla_{\mathbf{n}} \mu, \quad \mathbf{x} \in \partial\Omega, \\ \mu_s &= -\delta \Delta_s \phi + \frac{1}{\delta} g'(\phi) + \epsilon \nabla_{\mathbf{n}} \phi, \quad \mu = \beta \mu_s, \quad \mathbf{x} \in \partial\Omega, \\ \phi(\mathbf{x}, 0) &= \phi_0(\mathbf{x}), \quad \mathbf{x} \in \Omega \cup \partial\Omega, \end{aligned} \quad (1.10)$$

where $M_s^{(2)}$ is the mobility coefficient for the transport equation at the boundary. This model differs from the above model in the transport equation of ϕ at the boundary, where an Allen-Cahn equation is replaced by a surface Cahn-Hilliard equation. This modification results in the following mass equality

$$\beta \int_{\Omega} \phi(t) d\mathbf{x} + \int_{\partial\Omega} \phi(t) ds = \beta \int_{\Omega} \phi(0) d\mathbf{x} + \int_{\partial\Omega} \phi(0) ds, \quad (1.11)$$

where β can be viewed as a weight of the bulk mass compared to the surface mass.

The energy dissipation rate equation is given by

$$\frac{d}{dt} E = -M_b^{(2)} \int_{\Omega} |\nabla \mu|^2 d\mathbf{x} - M_s^{(2)} \int_{\partial\Omega} |\nabla_s \mu_s|^2 ds. \quad (1.12)$$

Note that this model differs from the Gal model in one dynamic boundary condition so that they yield different dynamics at the boundary and thereby different energy dissipation rates.

By setting $\nabla_{\mathbf{n}} \mu = 0$ instead of enforcing $\beta \mu_s = \mu$ at the boundary, Liu and Wu derived another set of boundary conditions for the Cahn-Hilliard model with dynamic boundary conditions (LW model) [40]:

$$\begin{aligned} \frac{\partial \phi}{\partial t} &= M_b^{(2)} \Delta \mu, \quad \mu = -\epsilon \Delta \phi + \frac{1}{\epsilon} f'(\phi), \quad \mathbf{x} \in \Omega, \\ \frac{\partial \phi}{\partial t} &= M_s^{(2)} \Delta_s \mu_s, \quad \mu_s = -\delta \Delta_s \phi + \frac{1}{\delta} g'(\phi) + \epsilon \nabla_{\mathbf{n}} \phi, \quad \nabla_{\mathbf{n}} \mu = 0, \quad \mathbf{x} \in \partial\Omega, \\ \phi(\mathbf{x}, 0) &= \phi_0(\mathbf{x}), \quad \mathbf{x} \in \Omega \cup \partial\Omega. \end{aligned} \quad (1.13)$$

In this model, mass conservation laws in the bulk and in the boundary are held respectively,

$$\int_{\Omega} \phi(\mathbf{x}, t) d\mathbf{x} = \int_{\Omega} \phi(\mathbf{x}, 0) d\mathbf{x}, \quad \int_{\partial\Omega} \phi(\mathbf{x}, t) ds = \int_{\partial\Omega} \phi(\mathbf{x}, 0) ds. \quad (1.14)$$

The energy dissipation rate is analogous to that in the GMS model, given by (1.12). This model dictates that there is no material loss through the boundary and the mass in the bulk and on the boundary are conserved, respectively, shown in (1.14). Although energy dissipation rates in these two models are identical, their numerical values may be different because of the difference in the dynamic boundary conditions.

In 2019, Knopf and Lam presented yet another set of dynamic boundary conditions for the Cahn-Hilliard equation by extending LW model at the boundary (KL model) [34]. The governing equation system and the boundary conditions are given by

$$\begin{aligned} \frac{\partial \phi}{\partial t} &= M_b^{(2)} \Delta \mu, \quad \mu = -\epsilon \Delta \phi + \frac{1}{\epsilon} f'(\phi), \quad \mathbf{x} \in \Omega, \\ \frac{\partial \psi}{\partial t} &= M_s^{(2)} \Delta_s \mu_s, \quad \mu_s = -\delta \Delta_s \psi + \frac{1}{\delta} g'(\psi) + \epsilon H'(\psi) \nabla_{\mathbf{n}} \phi, \quad \mathbf{x} \in \partial \Omega, \\ \epsilon K \nabla_{\mathbf{n}} \phi &= H(\psi) - \phi, \quad \nabla_{\mathbf{n}} \mu = 0, \quad \mathbf{x} \in \partial \Omega, \\ \phi(\mathbf{x}, 0) &= \phi_0(\mathbf{x}), \quad \mathbf{x} \in \Omega, \quad \psi(\mathbf{x}, 0) = \psi_0(\mathbf{x}), \quad \mathbf{x} \in \partial \Omega, \end{aligned} \quad (1.15)$$

where $H(\psi)$ is a prescribed function of ψ . The mass in the bulk and on the boundary are conserved respectively.

Here, a new function $H(\psi)$ is introduced into the chemical potential at the boundary surface. The modified free energy is given by

$$E = \int_{\Omega} \frac{\epsilon}{2} |\nabla \phi|^2 + \frac{1}{\epsilon} f(\phi) d\mathbf{x} + \int_{\partial \Omega} \left[\frac{\delta}{2} |\nabla_s \psi|^2 + \frac{1}{\delta} g(\psi) \right] ds + \int_{\partial \Omega} \frac{(H(\psi) - \phi)^2}{2K} ds, \quad (1.16)$$

If $K \rightarrow 0$ and $H(\psi) = \psi$, the KL model reduces to the LW model. The last term in the free energy is a term penalizing the difference between $H(\psi)$ and ϕ when $K \rightarrow 0$. Recently, Knopf and Signori derived nonlocal models with dynamic boundary conditions and analyzed their well-posedness [36], extending their work in this direction using distinct variables for the bulk and surface respectively.

In 2019, Knopf et al. derived a set of boundary conditions for the Cahn-Hilliard model (KLLM model) [35] as follows

$$\begin{aligned} \frac{\partial \phi}{\partial t} &= M_b^{(2)} \Delta \mu, \quad \mu = -\epsilon \Delta \phi + \frac{1}{\epsilon} f'(\phi), \quad \mathbf{x} \in \Omega, \\ \frac{\partial \phi}{\partial t} &= M_s^{(2)} \Delta_s \mu_s - \beta M \nabla_{\mathbf{n}} \mu, \quad \mu_s = -\delta \Delta_s \phi + \frac{1}{\delta} g'(\phi) + \epsilon \nabla_{\mathbf{n}} \phi, \quad \mathbf{x} \in \partial \Omega, \\ \alpha \nabla_{\mathbf{n}} \mu &= \beta \mu_s - \mu, \quad \mathbf{x} \in \partial \Omega, \\ \phi(\mathbf{x}, 0) &= \phi_0(\mathbf{x}), \quad \mathbf{x} \in \Omega \cup \partial \Omega, \end{aligned} \quad (1.17)$$

where α is a relaxation length parameter. Instead of forcing $\mu = \beta \mu_s$ or $\nabla_{\mathbf{n}} \mu = 0$ at the boundary, a relaxation mechanism is introduced along the external normal direction of the boundary via a Robin boundary condition on the chemical potential μ : $\alpha \nabla_{\mathbf{n}} \mu = \beta \mu_s - \mu$. This relaxation introduces an additional energy dissipation effect (term) to the energy dissipation rate:

$$\frac{d}{dt} E = -M_b^{(2)} \int_{\Omega} |\nabla \mu|^2 d\mathbf{x} - M_s^{(2)} \int_{\partial \Omega} |\nabla_s \mu_s|^2 ds - \frac{M_b^{(2)}}{\alpha} \int_{\partial \Omega} (\beta \mu_s - \mu)^2 ds. \quad (1.18)$$

The time rate of change of the total mass in the bulk and on the surface follows the same equation as (1.11).

Clearly, the dynamic boundary conditions in the above models are related, yielding different energy dissipation rates and mass conservation or transfer mechanisms between the bulk and the boundary. We briefly unwind the relations below.

- If $\beta \rightarrow \infty$ and $E_s = 0$, (1.17)-2 implies $\mu_s = 0$ and $\nabla_{\mathbf{n}}\phi = 0$. Analogously, if $\alpha \rightarrow \infty$, (1.17)-2 deuces $\nabla_{\mathbf{n}}\mu = 0$. So, the HNBC-CH Model can be viewed as a limiting case of the KLLM model.
- In (1.17)-2, $\beta\mu_s - \mu$ is explained as the difference of weighted surface chemical potential $\beta\mu_s$ and bulk chemical potential μ . We define $\frac{1}{\alpha}$ as the relaxation rate, the system reaches the "equilibrium" at $\beta\mu_s = \mu$ when $\alpha \rightarrow 0$. So, the KLLM model reduces to the GMS model at $\alpha = 0$.
- If $\alpha \rightarrow \infty$, there is no relaxation and mass transfer between the boundary and bulk, leading to $\nabla_{\mathbf{n}}\mu = 0$. Thus, the KLLM model reduces to the LW model.

In the analysis, we note that the KLLM model is a fairly general model which includes three others as special cases. However, it's not general enough to include the Gal Model and the KL model. Recently, Hao Wu reviewed the derivation and analysis of the classical Cahn-Hilliard equation with static and dynamic boundary condition [58]. In addition, all the above mentioned boundary conditions are valid in flat boundaries where the curvature vanishes. However, when the domain boundary has a non-negligible curvature, its can affect the dynamic boundary conditions. For arbitrarily shaped domain boundaries, we must include the curvature contribution to the boundary dynamics. In many real-world applications, the boundary of the materials domain is not flat and it has non-negligible curvature. When the curvature effect is taken into account, the dynamic boundary conditions alluded to earlier must be modified to take into account the important geometric effect. This study will attempt to address this issue for a family of free energies.

In addition, the above reviewed phase field models are for purely dissipative systems. There are analogous phase field models for systems that allow both irreversible and reversible processes. One class of the phase field models includes the inertia effect to allow wave propagation [21]. For example, the phase field model in [4] is given by

$$\phi_t = \nabla^2 \mu - \epsilon_0 \phi_{tt}, \quad \mu = -\nabla^2 \phi + f'(\phi) + \alpha_0 \phi_t, \quad \mathbf{x} \in \Omega, \quad (1.19)$$

where ϵ_0 is a measure of inertia and $\alpha_0 > 0$ is a viscosity coefficient. Apparently, there is an underlying unified framework available to derive models that are consistent with thermodynamical principles.

In this paper, we aim to develop such a general framework to derive thermodynamically consistent models together with boundary conditions for nonequilibrium materials systems in any domains with piecewise smooth boundaries, where boundary dynamics and the boundary curvature effect are fully accounted for. We derive the general dynamic boundary condition as a constitutive relation by applying the generalized Onsager principle at the boundary analogous to what one does in the bulk. We elaborate on two types of such dynamic boundary conditions specifically by prescribing two distinct energy dissipation mechanisms under the unified assumption that the mass flux at the boundary is dictated by the imbalance between the bulk chemical potential and the surface one. We show that most of the above reviewed boundary conditions are special cases of the two type boundary conditions. We illustrate the impact of boundary dynamics on the bulk structure using a phase field model for crystal growth in the end numerically.

The rest of the paper is organized as follows. In §2, we present a general model in domains with smooth boundaries, whose free energy depends on gradients of the phase field variable up to the second order, and discuss its various limits. In §3, we discuss the extension to phase field models with a general free energy with high order spatial derivative and a nonlocal free energy. In §4, we show the effect of surface dynamics on the crystal growth in a phase field model for crystal growth by numerical simulations. We summarize the results in §5.

2. Thermodynamically consistent phase field models with consistent dynamic boundary conditions

We present a general framework for deriving transport equations and consistent dynamic boundary conditions for a phase field model that yields a negative energy dissipation or a positive entropy production rate when all dynamics are accounted for. We illustrate the approach using the scalar phase field model for a binary material system with a free energy of up to second order spatial derivatives of the phase field variable. Then, we elucidate the path for extending it to the more general free energy functional including the nonlocal free energy later. We make contact with the models mentioned in the introduction by examining limiting cases of the model and showing that many of those models are special cases of the general model. We discuss the derivation in the isothermal case in this paper so that the free energy is the proper potential to work with.

2.1. Generalized Onsager principle

The classical Onsager linear response theory on which the Onsager principle for dissipative systems is based provides a viable way to calculate dissipative forces in relaxation dynamics in an irreversible nonequilibrium process [44–46]. In a general setting, the linear response theory states that given a chemical potential in an isothermal system, the generalized flux ϕ_t is proportional to the generalized force or chemical potential $\hat{\mu}$

$$\phi_t = -M\hat{\mu}, \quad (2.1)$$

where M is called the mobility. In general, M is an operator. For dissipative systems where dynamics are irreversible, the additional Onsager reciprocal relation dictates that M is symmetric; for conservative systems where dynamics are reversible, M is antisymmetric [56]. We note that when M is a differential operator, like in the Cahn-Hilliard equation system, the property of M is affected by the boundary conditions of the system. For a system where inertia is non-negligible and there coexist irreversible and reversible dynamics in the nonequilibrium process, we extend the force balance equation to a generalized Onsager principle [56, 61]

$$-M^{-1}\phi_t = \rho\phi_{tt} + \hat{\mu} \Leftrightarrow \phi_t = -M(\rho\phi_{tt} + \hat{\mu}), \quad (2.2)$$

where $\rho\phi_{tt}$ represents the inertia force, ρ is a measure of mass and M is the mobility operator which is not necessarily symmetric. We next use the generalized Onsager principle to derive the general phase field model along with its consistent boundary conditions for a binary material system.

2.2. Models with free energy of up to second spatial derivatives

Let the bulk free energy in a fixed material domain Ω be given by

$$E_b[\phi] = \int_{\Omega} e_b(\phi, \nabla\phi, \nabla\nabla\phi) d\mathbf{x}, \quad (2.3)$$

where e_b is the energy density per unit volume. We consider a binary material system with a boundary that may have its distinctive properties than the bulk and possesses its own surface energy of derivatives up to the second order in space

$$E_s[\phi] = \int_{\partial\Omega} e_s(\phi, \nabla_s\phi, \nabla_s\nabla_s\phi) ds, \quad (2.4)$$

where e_s is the surface energy density per unit area, the phase field variable in the surface energy density is defined by

$$\phi = \phi(\mathbf{x}, t)|_{\partial\Omega}, \quad (2.5)$$

and ∇_s is the surface gradient operator over piecewise smooth boundary $\partial\Omega$ as that in the introduction. We note that (2.5) is a critical assumption we adopt throughout the paper, which states that the phase field variable is continuous up to the boundary. The case where the phase field variable on the surface may not be the limit of the phase field variable in the bulk on the surface will be discussed in a sequel. Hence, we will not introduce a new notation for the phase field variable on the surface in this paper.

The free energy of the system is given by

$$E_f[\phi] = \int_{\Omega} e_b(\phi, \nabla\phi, \nabla\nabla\phi) d\mathbf{x} + \int_{\partial\Omega} e_s(\phi, \nabla_s\phi, \nabla_s\nabla_s\phi) ds. \quad (2.6)$$

We add the kinetic energy in the bulk and on the boundary to account for the inertia effect in the system such that the total free energy is given by

$$E[\phi] = \int_{\Omega} \left[\frac{\rho}{2} \phi_t^2 + e_b(\phi, \nabla\phi, \nabla\nabla\phi) \right] d\mathbf{x} + \int_{\partial\Omega} \left[\frac{\rho_s}{2} \phi_t^2 + e_s(\phi, \nabla_s\phi, \nabla_s\nabla_s\phi) \right] ds, \quad (2.7)$$

where ϕ_t is the invariant time derivative of ϕ , ρ and ρ_s are two mass densities that measure the inertia in the bulk and on the surface, respectively. We calculate the time rate of change of the free energy as follows, assuming domain Ω is fixed,

$$\begin{aligned} \frac{dE}{dt} &= \int_{\Omega} (\rho\phi_{tt} + \mu)\phi_t d\mathbf{x} + \int_{\partial\Omega} [\rho_s\phi_t\phi_{tt} + \frac{\partial e_s}{\partial\phi}\phi_t + \frac{\partial e_s}{\partial\nabla_s\phi}\nabla_s\phi_t + \frac{\partial e_s}{\partial\nabla_s\nabla_s\phi}\nabla_s\nabla_s\phi_t + \\ &\quad \mathbf{n} \cdot \frac{\partial e_b}{\partial\nabla\phi}\phi_t + \frac{\partial e_b}{\partial\nabla\nabla\phi} : \mathbf{n}\nabla\phi_t - \mathbf{n}\nabla : \frac{\partial e_b}{\partial\nabla\nabla\phi}\phi_t] ds \\ &= \int_{\Omega} (\rho\phi_{tt} + \mu)\phi_t d\mathbf{x} + \int_{\partial\Omega} [\rho_s\phi_t\phi_{tt} + \frac{\partial e_s}{\partial\phi}\phi_t - \nabla_s \cdot \frac{\partial e_s}{\partial\nabla_s\phi}\phi_t - 2H\mathbf{n} \cdot \frac{\partial e_s}{\partial\nabla_s\phi}\phi_t \\ &\quad - \nabla_s \cdot \frac{\partial e_s}{\partial\nabla_s\nabla_s\phi} \cdot \nabla_s\phi_t - 2H\mathbf{n} \cdot \frac{\partial e_s}{\partial\nabla_s\nabla_s\phi} \cdot \nabla_s\phi_t \\ &\quad + \mathbf{n} \cdot \frac{\partial e_b}{\partial\nabla\phi}\phi_t + \frac{\partial e_b}{\partial\nabla\nabla\phi} : \mathbf{n}\nabla\phi_t - (\mathbf{n}\nabla : \frac{\partial e_b}{\partial\nabla\nabla\phi})\phi_t] ds \\ &= \int_{\Omega} (\rho\phi_{tt} + \mu)\phi_t d\mathbf{x} + \int_{\partial\Omega} [\rho_s\phi_t\phi_{tt} + \mu_s\phi_t + \frac{\partial e_b}{\partial\nabla\nabla\phi} : \mathbf{nn}(\mathbf{n} \cdot \nabla\phi_t)] ds, \end{aligned} \quad (2.8)$$

where H is the mean curvature of the boundary, \mathbf{n} is the unit external normal of $\partial\Omega$, the bulk and surface chemical potential are given respectively by

$$\begin{aligned} \mu &= \frac{\partial e_b}{\partial\phi} - \nabla \cdot \frac{\partial e_b}{\partial\nabla\phi} + \nabla\nabla : \frac{\partial e_b}{\partial\nabla\nabla\phi}, \\ \mu_s &= \frac{\partial e_s}{\partial\phi} - \nabla_s \cdot \frac{\partial e_s}{\partial\nabla_s\phi} - 2H\mathbf{n} \cdot \frac{\partial e_s}{\partial\nabla_s\phi} + \mathbf{n} \cdot \frac{\partial e_b}{\partial\nabla\phi} - \mathbf{n}\nabla : \frac{\partial e_b}{\partial\nabla\nabla\phi} \\ &\quad + \nabla_s \nabla_s : \frac{\partial e_s}{\partial\nabla_s\nabla_s\phi} + 2H\mathbf{n}\nabla_s : \frac{\partial e_s}{\partial\nabla_s\nabla_s\phi} + \nabla_s \cdot (2H\mathbf{n} \cdot \frac{\partial e_s}{\partial\nabla_s\nabla_s\phi}) \\ &\quad + 4H^2\mathbf{nn} : \frac{\partial e_s}{\partial\nabla_s\nabla_s\phi} - \nabla_s\mathbf{n} : \frac{\partial e_b}{\partial\nabla\nabla\phi} - 2H\mathbf{nn} : \frac{\partial e_b}{\partial\nabla\nabla\phi}. \end{aligned} \quad (2.9)$$

Note that (i) the surface chemical potential includes contributions from the surface free energy as well as that from the bulk energy confined to the boundary; (ii) the mean curvature shows up in the surface chemical potential, indicating that curvature of the boundary affects the dynamics at the boundary; and (iii) more surface terms can appear if the free energy density function depends on higher order spatial derivatives. We adopt the Einstein notation for tensors, denote tensor product of vector \mathbf{n} and \mathbf{v} as $\mathbf{nv} = n_i v_j$, use one dot \cdot to represent inner product $\mathbf{n} \cdot \mathbf{v} = n_i v_i$ and two dots $:$ to represent contraction of two second order tensor $\mathbf{A} : \mathbf{C} = A_{ij} C_{ij}$, where \mathbf{n}, \mathbf{v} are vectors, \mathbf{A}, \mathbf{C} are second order tensors, and the Einstein notation is adopted.

2.2.1. Dynamics in the bulk

We apply the generalized Onsager principle firstly to the bulk integral in (2.8) to obtain the transport equation for ϕ in Ω

$$-M_b^{-1}\phi_t = \rho\phi_{tt} + \mu \Leftrightarrow \phi_t = -M_b(\rho\phi_{tt} + \mu), \quad \mathbf{x} \in \Omega, \quad (2.10)$$

where M_b is the mobility operator and M_b^{-1} is the friction operator which is positive semi-definite to ensure energy dissipation. We consider the mobility operator in the following form in this study

$$M_b = M_b^{(1)} - \nabla \cdot \mathbf{M}_b^{(2)} \cdot \nabla, \quad (2.11)$$

where $M_b^{(1)} \geq 0$ is a scalar function of ϕ and $\mathbf{M}_b^{(2)} \in \mathbf{R}^{3 \times 3}$ is a semi-definite positive matrix which can be a function of ϕ as well. If $\mathbf{M}_b^{(2)} = M_b^{(2)} \mathbf{I}$ and $M_b^{(2)}$ is also a scalar function of ϕ , then such a special case $\nabla \cdot \mathbf{M}_b^{(2)} \cdot \nabla = \nabla \cdot (M_b^{(2)} \nabla)$ can be obtained. We note that the derivation applies to a more general mobility operator with high order derivatives as well, which we will not pursue in this study. The presence of spatial derivatives in the mobility indicates the nonlocal interaction is accounted for in the friction operator M_b^{-1} . This is shown in the form of pseudo-differential operators. With this, the energy dissipation rate reduces to

$$\begin{aligned} \frac{dE}{dt} = & - \int_{\Omega} [(\mu + \rho\phi_{tt})M_b^{(1)}(\mu + \rho\phi_{tt}) + \nabla(\mu + \rho\phi_{tt}) \cdot \mathbf{M}_b^{(2)} \cdot \nabla(\mu + \rho\phi_{tt})] d\mathbf{x} \\ & + \int_{\partial\Omega} [(\mu_s + \rho_s\phi_{tt})\phi_t + \mu_c \nabla_{\mathbf{n}}\phi_t + (\mu + \rho\phi_{tt})\mathbf{n} \cdot \mathbf{M}_b^{(2)} \cdot \nabla(\mu + \rho\phi_{tt})] ds, \end{aligned} \quad (2.12)$$

where $\mu_c = \frac{\partial e_b}{\partial \nabla \nabla \phi} : \mathbf{nn}$. We denote the generalized chemical potential in the bulk by $\tilde{\mu} = \mu + \rho\phi_{tt}$ and in the surface by $\tilde{\mu}_s = \mu_s + \rho_s\phi_{tt}$, respectively. We remark that $\mathbf{n} \cdot \mathbf{M}_b^{(2)} \cdot \nabla(\mu + \rho\phi_{tt})$ is the inward mass flux across the boundary. This physical quantity is determined by the balance between the surface and bulk chemical potential. We next derive thermodynamically consistent boundary conditions.

2.2.2. Dynamics on boundaries

We first recognize that the boundary energy flux density is a quadratic form and then apply the Onsager principle the second time to the energy flux density to establish a dynamic constitutive equation at the boundary:

$$\begin{pmatrix} \phi_t \\ f_m \\ \nabla_{\mathbf{n}}\phi_t \end{pmatrix} = -M_{3 \times 3} \cdot \begin{pmatrix} \tilde{\mu}_s \\ \tilde{\mu} \\ \mu_c \end{pmatrix}, \quad (2.13)$$

where $f_m = \mathbf{n} \cdot \mathbf{M}_b^{(2)} \cdot \nabla \tilde{\mu}$ is the inward mass flux and $M_{3 \times 3} \geq 0$ is the surface mobility operator, a 3×3 matrix or second order tensor. $M_{3 \times 3} \geq 0$ means that its symmetric operator is semi-positive definite. Then,

$$\begin{aligned} \frac{dE}{dt} = & - \int_{\Omega} [\tilde{\mu} M_b^{(1)} \tilde{\mu} + \nabla \tilde{\mu} \cdot \mathbf{M}_b^{(2)} \cdot \nabla \tilde{\mu}] d\mathbf{x} \\ & - \int_{\partial\Omega} [(\tilde{\mu}_s, \tilde{\mu}, \mu_c)(M_{3 \times 3})(\tilde{\mu}_s, \tilde{\mu}, \mu_c)^T] ds \leq 0, \end{aligned} \quad (2.14)$$

which indicates the system is dissipative. We examine two special cases that include most of the models and boundary conditions mentioned in the introduction below.

Case 1: a purely dissipative boundary condition.

We define a symmetric mobility operator as follows

$$M_{3 \times 3} = \begin{pmatrix} M_s + \frac{\beta^2}{\alpha} & -\frac{\beta}{\alpha} & 0 \\ -\frac{\beta}{\alpha} & \frac{1}{\alpha} & 0 \\ 0 & 0 & M_c \end{pmatrix}, \quad (2.15)$$

where M_s is a semi-definite positive operator, $\alpha \geq 0$ is a friction coefficient, $1/\beta \geq 0$ is a length parameter, and M_c is a semi-definite positive mobility operator. We note that these mobility operators can be differential operators. When M_c is a scalar in a simple example and $M_c \rightarrow \infty$, $\mu_c = \frac{\partial e_b}{\partial \nabla \nabla \phi} : \mathbf{nn} = 0$; while $M_c \rightarrow 0$, $\nabla_{\mathbf{n}} \phi_t = 0$.

This constitutive equation establishes a balance between the inward mass flux at the boundary and the generalized chemical potential difference between the bulk and the surface: it assumes the inward mass flux is proportional to the difference between the chemical potential in the bulk and the weighted one at the boundary. When the weighted surface energy is higher than the bulk energy confined to the boundary, the mass flux is inward; otherwise, the mass flux flows outward. In either case, the total energy dissipates when $M_{3 \times 3} \geq 0$.

The governing equation together with the boundary conditions in this model is given as follows

$$\begin{aligned} \frac{\partial \phi}{\partial t} &= -M_b \tilde{\mu}, \quad \mathbf{x} \in \Omega, \\ \frac{\partial \phi}{\partial t} &= -(M_s + \frac{\beta^2}{\alpha}) \tilde{\mu}_s + \frac{\beta}{\alpha} \tilde{\mu}, \quad \mathbf{x} \in \partial\Omega, \\ \alpha \mathbf{n} \cdot \mathbf{M}_b^{(2)} \cdot \nabla \tilde{\mu} &= -\tilde{\mu} + \beta \tilde{\mu}_s, \quad \nabla_{\mathbf{n}} \phi_t = -M_c \mu_c, \quad \mathbf{x} \in \partial\Omega, \\ \phi(0) &= \phi_0, \quad \mathbf{x} \in \Omega \cup \partial\Omega. \end{aligned} \quad (2.16)$$

The corresponding energy dissipation rate is given by

$$\begin{aligned} \frac{dE}{dt} &= - \int_{\Omega} [\tilde{\mu} M_b^{(1)} \tilde{\mu} + \nabla \tilde{\mu} \cdot \mathbf{M}_b^{(2)} \cdot \nabla \tilde{\mu}] d\mathbf{x} - \int_{\partial\Omega} [\mu_c M_c \mu_c] ds \\ &\quad + \int_{\partial\Omega} [\tilde{\mu}_s (\phi_t + \beta \mathbf{n} \cdot \mathbf{M}_b^{(2)} \cdot \nabla \tilde{\mu})] ds - \frac{1}{\alpha} \int_{\partial\Omega} (\beta \tilde{\mu}_s - \tilde{\mu})^2 ds. \end{aligned} \quad (2.17)$$

The surface transport equation of ϕ can be rewritten into an alternative form on boundary $\partial\Omega$

$$\frac{\partial \phi}{\partial t} = -M_s \tilde{\mu}_s - \beta f_m, \quad \mathbf{x} \in \partial\Omega, \quad (2.18)$$

where

$$f_m = \mathbf{n} \cdot \mathbf{M}_b^{(2)} \cdot \nabla \tilde{\mu} = \frac{1}{\alpha} (\beta \tilde{\mu}_s - \tilde{\mu}). \quad (2.19)$$

This indicates that the time rate of change of mass fraction ϕ is proportional to the outward mass flux and the generalized surface chemical potential.

Case 2: a dissipative and transportive boundary condition

In the second case, we propose another mobility operator as follows

$$M_{3 \times 3} = \begin{pmatrix} M_s & \frac{\beta}{\alpha} & 0 \\ -\frac{\beta}{\alpha} & \frac{1}{\alpha} & 0 \\ 0 & 0 & M_c \end{pmatrix} = \begin{pmatrix} M_s & 0 & 0 \\ 0 & \frac{1}{\alpha} & 0 \\ 0 & 0 & M_c \end{pmatrix} + \begin{pmatrix} 0 & \frac{\beta}{\alpha} & 0 \\ -\frac{\beta}{\alpha} & 0 & 0 \\ 0 & 0 & 0 \end{pmatrix}, \quad (2.20)$$

which includes an antisymmetric component, contributing to transport dynamics at the boundary, in addition to the positive semi-definite operator in $M_{3 \times 3}$. The antisymmetric mobility component represents an energy exchange between the bulk and the boundary without inducing any dissipation.

The governing equation together with the boundary conditions in this model is summarized as follows

$$\begin{aligned}
\frac{\partial \phi}{\partial t} &= -M_b \tilde{\mu}, \quad \mathbf{x} \in \Omega, \\
\frac{\partial \phi}{\partial t} &= -M_s \tilde{\mu}_s - \frac{\beta}{\alpha} \tilde{\mu}, \quad \mathbf{x} \in \partial\Omega, \\
\alpha \mathbf{n} \cdot \mathbf{M}_b^{(2)} \cdot \nabla \tilde{\mu} &= -\tilde{\mu} + \beta \tilde{\mu}_s, \quad \nabla_{\mathbf{n}} \phi_t = -M_c \mu_c, \quad \mathbf{x} \in \partial\Omega, \\
\phi(\mathbf{x}, 0) &= \phi_0, \quad \mathbf{x} \in \Omega \cup \partial\Omega.
\end{aligned} \tag{2.21}$$

Notice that the mobility matrix has an antisymmetric component which does not contribute to the energy dissipation. This set of boundary conditions has the following interpretation: the time rate of change of the phase field variable at the boundary is proportional to both the surface chemical potential and the inward flux across the boundary.

The corresponding energy dissipation rate is given by

$$\frac{dE}{dt} = - \int_{\Omega} [\tilde{\mu} M_b^{(1)} \tilde{\mu} + \nabla \tilde{\mu} \cdot \mathbf{M}_b^{(2)} \cdot \nabla \tilde{\mu}] d\mathbf{x} - \int_{\partial\Omega} [\tilde{\mu}_s M_s \tilde{\mu}_s + \frac{1}{\alpha} \tilde{\mu}^2 + \mu_c M_c \mu_c] ds. \tag{2.22}$$

The two types of dynamic boundary conditions are derived from two different considerations of the mobility operator, which contribute to distinct energy dissipation mechanisms, following the generalized Onsager principle under a unified assumption that the boundary mass flux is proportional to the difference of the bulk energy confined at the boundary and a weighted surface energy. In the first case, the time rate of change of mass fraction (phase field variable) is proportional to the surface chemical potential and the outward mass flux. As a result, the distinctive surface energy dissipation rate is directly linked to the magnitude of the mass flux across the boundary surface. In the second case, the time rate of change of mass fraction is proportional to the surface chemical potential and the inward mass flux. Consequentially, the distinctive surface energy dissipation rate is measured by the bulk chemical potential confined to the surface. Two different dissipative mechanisms define two different dynamic models at the boundary. There are more cases that one can elaborate on by specifying specific form of operator $M_{3 \times 3}$, which we will not enumerate in this study.

In general, mobility operator in the bulk $M_b = M_b^{sym} + M_b^{anti}$ in (2.2) can be decomposed into symmetric and antisymmetric part, where M_b^{sym} is semi-definite positive. There can be many more thermodynamically consistent boundary conditions that are compatible to the given bulk transport equation. For the mobility operators at the boundary, we consider the following forms, analogously to the bulk,

$$M_s = M_s^{(1)} - \nabla_s \cdot \mathbf{M}_s^{(2)} \cdot \nabla_s, \quad M_c = M_c^{(1)} - \nabla_s \cdot \mathbf{M}_c^{(2)} \cdot \nabla_s, \tag{2.23}$$

where $M_c^{(1)} \geq 0$, $M_s^{(1)} \geq 0$, and $\mathbf{M}_s^{(2)}$ and $\mathbf{M}_c^{(2)}$ are 3×3 positive semi-definite matrices. Then,

$$\begin{aligned}
- \int_{\partial\Omega} [\tilde{\mu}_s M_s \tilde{\mu}_s] ds &= - \int_{\partial\Omega} [\tilde{\mu}_s M_s^{(1)} \tilde{\mu}_s + \nabla_s \tilde{\mu}_s \cdot \mathbf{M}_s^{(2)} \cdot \nabla_s \tilde{\mu}_s] ds \\
- \int_{\partial\Omega} [2H \tilde{\mu}_s \mathbf{n} \cdot \mathbf{M}_s^{(2)} \cdot \nabla_s \tilde{\mu}_s] ds,
\end{aligned} \tag{2.24}$$

$$\begin{aligned}
- \int_{\partial\Omega} [\mu_c M_c \mu_c] ds &= - \int_{\partial\Omega} [\mu_c M_c^{(1)} \mu_c + \nabla_s \mu_c \cdot \mathbf{M}_c^{(2)} \cdot \nabla_s \mu_c] ds \\
- \int_{\partial\Omega} [2H \mu_c \mathbf{n} \cdot \mathbf{M}_c^{(2)} \cdot \nabla_s \mu_c] ds.
\end{aligned} \tag{2.25}$$

Whether or not the energy dissipation rate at the boundary is nonpositive depends on the last terms in (2.24) and (2.25), which are linearly proportional to the mean curvature.

If $\mathbf{M}_s^{(2)} = M_s^{(2)} \mathbf{I}$ and $\mathbf{M}_c^{(2)} = M_c^{(2)} \mathbf{I}$, where $M_s^{(2)} \geq 0$ and $M_c^{(2)} \geq 0$ are scalar functions of ϕ , the last terms in (2.24) and (2.25) vanish and the energy dissipation rate at the boundary are nonpositive due to $\mathbf{n} \cdot \nabla_s \mu_s = \mathbf{n} \cdot \nabla_s \mu_c = 0$. Of course, $H = 0$ is also a sufficient condition for non-positive energy dissipation rates.

It follows from (2.16) that

$$\begin{aligned} & \frac{d}{dt} [\int_{\Omega} \beta \phi d\mathbf{x} + \int_{\partial\Omega} \phi ds] \\ & = -\beta \int_{\Omega} M_b^{(1)} \tilde{\mu} d\mathbf{x} - \int_{\partial\Omega} [M_s^{(1)} \tilde{\mu}_s + 2H \mathbf{n} \cdot \mathbf{M}_s^{(2)} \cdot \nabla_s \tilde{\mu}_s] ds. \end{aligned} \quad (2.26)$$

If $\mathbf{M}_s^{(2)} = M_s^{(2)} \mathbf{I}$ or $H = 0$,

$$\frac{d}{dt} [\int_{\Omega} \beta \phi d\mathbf{x} + \int_{\partial\Omega} \phi ds] = -\beta \int_{\Omega} M_b^{(1)} \tilde{\mu} d\mathbf{x} - \int_{\partial\Omega} M_s^{(1)} \tilde{\mu}_s ds. \quad (2.27)$$

If $M_b^{(1)} = 0, M_s^{(1)} = 0$,

$$\frac{d}{dt} [\int_{\Omega} \beta \phi d\mathbf{x} + \int_{\partial\Omega} \phi ds] = 0. \quad (2.28)$$

This indicates a weighted mass in the bulk and the mass over the surface is conserved under this dynamic boundary condition. In this case, parameter β in the dynamic boundary condition can be interpreted as the weighted mass at the bulk to that over the surface.

Model (2.16) and (2.21) give a general phase field model with two different dynamic boundary conditions, where the surface transport equation of ϕ at the boundary sets the two models apart. In the first one, the across boundary mass flux contributes directly to the energy dissipation on the surface; while in the second, it is the bulk chemical potential limited to the boundary contributes to the energy dissipation on the surface directly. We next examine various limiting cases to show that most models mentioned in the introduction are special cases of model (2.16) and (2.21), respectively. Specifically, when the across boundary mass flux is forbidden, i.e., $\alpha = \infty$ and $\beta = 0$, we show that the two types of dynamic boundary conditions are identical.

2.3. Limiting cases

Since (2.16) and (2.21) describe two different dynamics at the boundary, we examine them closely in several limiting cases and make contact with the models alluded to in the introduction and in the literature. Notice that when $\rho = \rho_s = 0$, the phase field model reduces to the over-damped limit where the inertia force is neglected, $\tilde{\mu} = \mu$ and $\tilde{\mu}_s = \mu_s$. We present limits of the under-damped case in the following, the results for the over-damped ones are obtained by setting $\rho = \rho_s = 0$.

- Let $\beta \rightarrow 0$, the boundary conditions reduce to

$$\alpha \mathbf{n} \cdot \mathbf{M}_b^{(2)} \cdot \nabla \tilde{\mu} = -\tilde{\mu}, \quad \phi_t = -M_s \tilde{\mu}_s, \quad \nabla_{\mathbf{n}} \phi_t = -M_c \mu_c, \quad \mathbf{x} \in \partial\Omega. \quad (2.29)$$

The first equation states that the mass flux between the bulk and the boundary is completely dictated by the bulk chemical potential extrapolated (or confined) to the boundary. The second one shows the relaxation dynamics of mass fraction at the surface are dictated completely by the surface chemical potential. This indicates that the across boundary mass flux does not interfere with the surface dynamics at the boundary. The third one is necessary only when the free energy has second order spatial derivatives, which represents the relaxation dynamics of the directional derivative of the volume fraction.

Then the energy dissipation rate reduces to

$$\begin{aligned} \frac{dE}{dt} &= - \int_{\Omega} [\tilde{\mu} M_b^{(1)} \tilde{\mu} + \nabla \tilde{\mu} \cdot \mathbf{M}_b^{(2)} \cdot \nabla \tilde{\mu}] d\mathbf{x} - \int_{\partial\Omega} [\tilde{\mu}_s M_s \tilde{\mu}_s] ds \\ &\quad - \int_{\partial\Omega} [\frac{1}{\alpha} \tilde{\mu}^2 + \mu_c M_c \mu_c] ds \leq 0. \end{aligned} \quad (2.30)$$

Model (2.16) and (2.21) are identical and dissipative in this limit.

- Limit $\alpha \rightarrow 0$ is a singular limit. We will conduct the limiting process in the following order. Firstly, we substitute (2.16)-3 into (2.16)-2; secondly, we take the limit $\alpha \rightarrow 0$ in (2.16)-3. The results are given by

$$\begin{aligned} \phi_t + \beta \mathbf{n} \cdot \mathbf{M}_b^{(2)} \cdot \nabla \tilde{\mu} &= -M_s \tilde{\mu}_s, \quad \mathbf{x} \in \partial\Omega, \\ \beta \tilde{\mu}_s &= \tilde{\mu}, \quad \nabla_{\mathbf{n}} \phi_t = -M_c \mu_c, \quad \mathbf{x} \in \partial\Omega. \end{aligned} \quad (2.31)$$

These conditions state that the bulk chemical potential and the weighted surface one reach a balance at the boundary and the time rate of change in the phase field variable at the boundary is given by the rate of change due to the outward mass flux and the surface chemical potential. The energy dissipation rate reduces to

$$\begin{aligned} \frac{dE}{dt} &= - \int_{\Omega} [\tilde{\mu} M_b^{(1)} \tilde{\mu} + \nabla \tilde{\mu} \cdot \mathbf{M}_b^{(2)} \cdot \nabla \tilde{\mu}] d\mathbf{x} - \int_{\partial\Omega} [\tilde{\mu}_s M_s \tilde{\mu}_s] ds \\ &\quad - \int_{\partial\Omega} [\mu_c M_c \mu_c] ds. \end{aligned} \quad (2.32)$$

The model is dissipative with the boundary conditions.

If we take the singular limit in (2.21), we end up with

$$\tilde{\mu} = 0, \quad \tilde{\mu}_s = 0, \quad \nabla_{\mathbf{n}} \phi_t = -M_c \mu_c, \quad \mathbf{x} \in \partial\Omega. \quad (2.33)$$

and the energy dissipation rate is given by

$$\frac{dE}{dt} = - \int_{\Omega} [\tilde{\mu} M_b^{(1)} \tilde{\mu} + \nabla \tilde{\mu} \cdot \mathbf{M}_b^{(2)} \cdot \nabla \tilde{\mu}] d\mathbf{x} - \int_{\partial\Omega} [\mu_c M_c \mu_c] ds. \quad (2.34)$$

The two models do not give the same set of boundary conditions. They indeed describe two different dynamics in the limit.

- When $\alpha \rightarrow \infty$, we have

$$\phi_t = -M_s \tilde{\mu}_s, \quad \mathbf{n} \cdot \mathbf{M}_b^{(2)} \cdot \nabla \tilde{\mu} = 0, \quad \nabla_{\mathbf{n}} \phi_t = -M_c \mu_c, \quad \mathbf{x} \in \partial\Omega, \quad (2.35)$$

and the energy dissipation rate is given by (2.32). The boundary conditions stipulate that the mass flux at the boundary vanishes and the phase field dynamics at the boundary is dictated by relaxation dynamics of the surface mass fraction exclusively. The two models are once again identical and dissipative.

We summarize the dynamic boundary conditions and energy dissipation rates in table 2.1 and 2.2 in the limits. In the case $\alpha \rightarrow 0$, the two models are not identical, whereas they are the same in the other two cases. While both α and β are finite, we consider the limiting cases with respect to boundary mobility operators M_s and M_c , respectively. The results are tabulated in tables 2.3 and 2.4, respectively. Regardless what are the surface mobility operators, the two boundary conditions are different in the cases, yielding two distinct thermodynamically consistent phase field models with consistent dynamic boundary conditions. Note that the two dynamic boundary conditions differ in how the mass flux transfers across the boundary and how mass fraction dynamics on the surface are prescribed. In table 2.5, we demonstrate that most

existing models mentioned in the introduction are special cases of the general model with the first type dynamic boundary condition. It is obvious that none of these models are the special case of the general model with the second type dynamic boundary condition. In fact, there are also some progresses in the nonlocal model with dynamic boundary conditions recently [36], which is also a special case of the general model with first type of dynamic boundary condition. We discuss the general nonlocal models with two types of dynamic boundary conditions in the next section. Notice that models (2.16) and (2.21) include all the models alluded to in the introduction as special cases except for the KL model when the free energy is limited to functionals of up to the first order spatial derivative. This is shown clearly in Table 2.5. Thus, the phase field model presented here is indeed a general phase field model. Moreover, the boundary conditions derived in this study include the curvature effect for an arbitrarily shaped piecewise smooth boundary, which have not been considered in previous studies. Finally, we note that any set of boundary conditions delineated here or their limiting cases may appear as boundary conditions on a smooth piece of the piecewise smooth boundary so that the overall boundary conditions can be a combination of the sets of dynamic boundary conditions.

Case	I	II
$\beta \rightarrow 0$	$\frac{\partial \phi}{\partial t} = -M_s \tilde{\mu}_s, \quad \alpha \mathbf{n} \cdot \mathbf{M}_b^{(2)} \cdot \nabla \tilde{\mu} = -\tilde{\mu}, \quad \nabla_{\mathbf{n}} \phi_t = -M_c \mu_c$	
$\alpha \rightarrow 0$	$\frac{\partial \phi}{\partial t} + \beta \mathbf{n} \cdot \mathbf{M}_b^{(2)} \cdot \tilde{\mu} = -M_s \tilde{\mu}_s, \quad \beta \tilde{\mu}_s = \tilde{\mu}, \quad \nabla_{\mathbf{n}} \phi_t = -M_c \mu_c$	$\tilde{\mu} = 0, \quad \tilde{\mu}_s = 0, \quad \nabla_{\mathbf{n}} \phi_t = -M_c \mu_c$
$\alpha \rightarrow \infty$	$\frac{\partial \phi}{\partial t} = -M_s \tilde{\mu}_s, \quad \mathbf{n} \cdot \mathbf{M}_b^{(2)} \cdot \nabla \tilde{\mu} = 0, \quad \nabla_{\mathbf{n}} \phi_t = -M_c \mu_c$	

TABLE 2.1. Dynamical boundary conditions in three limiting cases.

Case	I
$\beta \rightarrow 0$	$\frac{dE}{dt} = - \int_{\Omega} [\tilde{\mu} M_b^{(1)} \tilde{\mu} + \nabla \tilde{\mu} \cdot \mathbf{M}_b^{(2)} \cdot \nabla \tilde{\mu}] d\mathbf{x} - \int_{\partial\Omega} [\tilde{\mu}_s M_s \tilde{\mu}_s] ds - \frac{1}{\alpha} \int_{\partial\Omega} [\tilde{\mu}^2] ds - \int_{\partial\Omega} [\mu_c M_c \mu_c] ds$
$\alpha \rightarrow 0$	$\frac{dE}{dt} = - \int_{\Omega} [\tilde{\mu} M_b^{(1)} \tilde{\mu} + \nabla \tilde{\mu} \cdot \mathbf{M}_b^{(2)} \cdot \nabla \tilde{\mu}] d\mathbf{x} - \int_{\partial\Omega} [\tilde{\mu}_s M_s \tilde{\mu}_s + \mu_c M_c \mu_c] ds$
$\alpha \rightarrow \infty$	$\frac{dE}{dt} = - \int_{\Omega} [\tilde{\mu} M_b^{(1)} \tilde{\mu} + \nabla \tilde{\mu} \cdot \mathbf{M}_b^{(2)} \cdot \nabla \tilde{\mu}] d\mathbf{x} - \int_{\partial\Omega} [\tilde{\mu}_s M_s \tilde{\mu}_s] ds - \int_{\partial\Omega} [\mu_c M_c \mu_c] ds$
Case	II
$\beta \rightarrow 0$	$\frac{dE}{dt} = - \int_{\Omega} [\tilde{\mu} M_b^{(1)} \tilde{\mu} + \nabla \tilde{\mu} \cdot \mathbf{M}_b^{(2)} \cdot \nabla \tilde{\mu}] d\mathbf{x} - \int_{\partial\Omega} [\tilde{\mu}_s M_s \tilde{\mu}_s] ds - \frac{1}{\alpha} \int_{\partial\Omega} [\tilde{\mu}^2] ds - \int_{\partial\Omega} [\mu_c M_c \mu_c] ds$
$\alpha \rightarrow 0$	$\frac{dE}{dt} = - \int_{\Omega} [\tilde{\mu} M_b^{(1)} \tilde{\mu} + \nabla \tilde{\mu} \cdot \mathbf{M}_b^{(2)} \cdot \nabla \tilde{\mu}] d\mathbf{x} - \int_{\partial\Omega} [\mu_c M_c \mu_c] ds$
$\alpha \rightarrow \infty$	$\frac{dE}{dt} = - \int_{\Omega} [\tilde{\mu} M_b^{(1)} \tilde{\mu} + \nabla \tilde{\mu} \cdot \mathbf{M}_b^{(2)} \cdot \nabla \tilde{\mu}] d\mathbf{x} - \int_{\partial\Omega} [\tilde{\mu}_s M_s \tilde{\mu}_s] ds - \int_{\partial\Omega} [\mu_c M_c \mu_c] ds$

TABLE 2.2. Energy dissipation rates in three limiting cases. I and II represent the first and second type of boundary condition, respectively, when they are different.

Case	I
$M_s \rightarrow 0$	$\frac{\partial \phi}{\partial t} = -\frac{\beta^2}{\alpha} \tilde{\mu}_s + \frac{\beta}{\alpha} \tilde{\mu}, \quad \alpha \mathbf{n} \cdot \mathbf{M}_b^{(2)} \cdot \nabla \tilde{\mu} = \beta \tilde{\mu}_s - \tilde{\mu}, \quad \nabla_{\mathbf{n}} \phi_t = -M_c \mu_c$
$M_s \rightarrow \infty$	$\frac{\partial \phi}{\partial t} = -\beta \mathbf{n} \cdot \mathbf{M}_b^{(2)} \cdot \nabla \tilde{\mu}, \quad \tilde{\mu}_s = 0, \quad \nabla_{\mathbf{n}} \phi_t = -M_c \mu_c$
$M_c \rightarrow 0$	$\frac{\partial \phi}{\partial t} = -(M_s + \frac{\beta^2}{\alpha}) \tilde{\mu}_s + \frac{\beta}{\alpha} \tilde{\mu}, \quad \alpha \mathbf{n} \cdot \mathbf{M}_b^{(2)} \cdot \nabla \tilde{\mu} = \beta \tilde{\mu}_s - \tilde{\mu}, \quad \nabla_{\mathbf{n}} \phi_t = 0$
$M_c \rightarrow \infty$	$\frac{\partial \phi}{\partial t} = -(M_s + \frac{\beta^2}{\alpha}) \tilde{\mu}_s + \frac{\beta}{\alpha} \tilde{\mu}, \quad \alpha \mathbf{n} \cdot \mathbf{M}_b^{(2)} \cdot \nabla \tilde{\mu} = \beta \tilde{\mu}_s - \tilde{\mu}, \quad \mu_c = 0$
Case	II
$M_s \rightarrow 0$	$\frac{\partial \phi}{\partial t} = -\frac{\beta}{\alpha} \tilde{\mu}, \quad \alpha \mathbf{n} \cdot \mathbf{M}_b^{(2)} \cdot \nabla \tilde{\mu} = \beta \tilde{\mu}_s - \tilde{\mu}, \quad \nabla_{\mathbf{n}} \phi_t = -M_c \mu_c$
$M_s \rightarrow \infty$	$\frac{\partial \phi}{\partial t} = \beta \mathbf{n} \cdot \mathbf{M}_b^{(2)} \cdot \nabla \tilde{\mu}, \quad \tilde{\mu}_s = 0, \quad \nabla_{\mathbf{n}} \phi_t = -M_c \mu_c$
$M_c \rightarrow 0$	$\frac{\partial \phi}{\partial t} = -M_s \tilde{\mu}_s - \frac{\beta}{\alpha} \tilde{\mu}, \quad \alpha \mathbf{n} \cdot \mathbf{M}_b^{(2)} \cdot \nabla \tilde{\mu} = \beta \tilde{\mu}_s - \tilde{\mu}, \quad \nabla_{\mathbf{n}} \phi_t = 0$
$M_c \rightarrow \infty$	$\frac{\partial \phi}{\partial t} = -M_s \tilde{\mu}_s - \frac{\beta}{\alpha} \tilde{\mu}, \quad \alpha \mathbf{n} \cdot \mathbf{M}_b^{(2)} \cdot \nabla \tilde{\mu} = \beta \tilde{\mu}_s - \tilde{\mu}, \quad \mu_c = 0$

TABLE 2.3. Two types of dynamic boundary conditions.

Case	I
$M_s \rightarrow 0$	$\frac{dE}{dt} = -\int_{\Omega} [\tilde{\mu} M_b^{(1)} \tilde{\mu} + \nabla \tilde{\mu} \cdot \mathbf{M}_b^{(2)} \cdot \nabla \tilde{\mu}] d\mathbf{x} - \frac{1}{\alpha} \int_{\partial\Omega} [(\beta \tilde{\mu}_s - \tilde{\mu})^2] ds - \int_{\partial\Omega} [\mu_c M_c \mu_c] ds$
$M_s \rightarrow \infty$	$\frac{dE}{dt} = -\int_{\Omega} [\tilde{\mu} M_b^{(1)} \tilde{\mu} + \nabla \tilde{\mu} \cdot \mathbf{M}_b^{(2)} \cdot \nabla \tilde{\mu}] d\mathbf{x} - \frac{1}{\alpha} \int_{\partial\Omega} [\tilde{\mu}^2] ds - \int_{\partial\Omega} [\mu_c M_c \mu_c] ds$
$M_c \rightarrow 0$	$\frac{dE}{dt} = -\int_{\Omega} [\tilde{\mu} M_b^{(1)} \tilde{\mu} + \nabla \tilde{\mu} \cdot \mathbf{M}_b^{(2)} \cdot \nabla \tilde{\mu}] d\mathbf{x} - \int_{\partial\Omega} [\tilde{\mu}_s M_s \tilde{\mu}_s] ds - \frac{1}{\alpha} \int_{\partial\Omega} [(\beta \tilde{\mu}_s - \tilde{\mu})^2] ds$
$M_c \rightarrow \infty$	$\frac{dE}{dt} = -\int_{\Omega} [\tilde{\mu} M_b^{(1)} \tilde{\mu} + \nabla \tilde{\mu} \cdot \mathbf{M}_b^{(2)} \cdot \nabla \tilde{\mu}] d\mathbf{x} - \int_{\partial\Omega} [\tilde{\mu}_s M_s \tilde{\mu}_s] ds - \frac{1}{\alpha} \int_{\partial\Omega} [(\beta \tilde{\mu}_s - \tilde{\mu})^2] ds$
Case	II
$M_s \rightarrow 0$	$\frac{dE}{dt} = -\int_{\Omega} [\tilde{\mu} M_b^{(1)} \tilde{\mu} + \nabla \tilde{\mu} \cdot \mathbf{M}_b^{(2)} \cdot \nabla \tilde{\mu}] d\mathbf{x} - \frac{1}{\alpha} \int_{\partial\Omega} [\tilde{\mu}^2] ds - \int_{\partial\Omega} [\mu_c M_c \mu_c] ds$
$M_s \rightarrow \infty$	$\frac{dE}{dt} = -\int_{\Omega} [\tilde{\mu} M_b^{(1)} \tilde{\mu} + \nabla \tilde{\mu} \cdot \mathbf{M}_b^{(2)} \cdot \nabla \tilde{\mu}] d\mathbf{x} - \frac{1}{\alpha} \int_{\partial\Omega} [\tilde{\mu}^2] ds - \int_{\partial\Omega} [\mu_c M_c \mu_c] ds$
$M_c \rightarrow 0$	$\frac{dE}{dt} = -\int_{\Omega} [\tilde{\mu} M_b^{(1)} \tilde{\mu} + \nabla \tilde{\mu} \cdot \mathbf{M}_b^{(2)} \cdot \nabla \tilde{\mu}] d\mathbf{x} - \int_{\partial\Omega} \tilde{\mu}_s M_s \tilde{\mu}_s ds - \frac{1}{\alpha} \int_{\partial\Omega} [\tilde{\mu}^2] ds$
$M_c \rightarrow \infty$	$\frac{dE}{dt} = -\int_{\Omega} [\tilde{\mu} M_b^{(1)} \tilde{\mu} + \nabla \tilde{\mu} \cdot \mathbf{M}_b^{(2)} \cdot \nabla \tilde{\mu}] d\mathbf{x} - \int_{\partial\Omega} \tilde{\mu}_s M_s \tilde{\mu}_s ds - \frac{1}{\alpha} \int_{\partial\Omega} [\tilde{\mu}^2] ds$

TABLE 2.4. The free energy dissipation rates corresponding to the two types of boundary dynamics.

Models	Specific conditions for the model with first type of dynamic boundary condition
Gal model [18]	$M_b = M_b^{(2)} \nabla^2, \quad M_s = 1, \quad \alpha = 0, \quad \rho = \rho_s = \mu_c = M_c = H = 0$
GMS model [26]	$M_b = M_b^{(2)} \nabla^2, \quad M_s = M_s^{(2)} \nabla_s^2, \quad \alpha = 0, \quad \rho = \rho_s = \mu_c = M_c = H = 0$
LW model [40]	$M_b = M_b^{(2)} \nabla^2, \quad M_s = M_s^{(2)} \nabla_s^2, \quad \alpha \rightarrow \infty, \quad \rho = \rho_s = \mu_c = M_c = H = 0$
KLLM model [35]	$M_b = M_b^{(2)} \nabla^2, \quad M_s = M_s^{(2)} \nabla_s^2, \quad \rho = \rho_s = \mu_c = M_c = H = 0$

TABLE 2.5. Relation between the general model with first types of dynamic boundary conditions and several existing models in the literature.

2.4. Mixed dynamic boundary conditions

Let us consider a domain Ω with piecewise smooth boundaries $\partial\Omega = \cup_{i=1}^N \Gamma_i$, where Γ_i and Γ_j are either mutually disjoint or adjacent smooth surfaces, $i, j = 1, \dots, N$. The energy dissipation rate in (2.12) can be rewritten into

$$\begin{aligned} \frac{dE}{dt} = & - \int_{\Omega} [\tilde{\mu} M_b^{(1)} \tilde{\mu} + \nabla \tilde{\mu} \cdot \mathbf{M}_b^{(2)} \cdot \nabla \tilde{\mu}] d\mathbf{x} \\ & + \sum_{i=1}^N \int_{\Gamma_i} [\tilde{\mu}_s \phi_t + \mu_c \mathbf{n} \cdot \nabla \phi_t + \tilde{\mu} \mathbf{n} \cdot \mathbf{M}_b^{(2)} \cdot \nabla \tilde{\mu}] ds. \end{aligned} \quad (2.36)$$

For the surface terms in (2.36), either of two boundary conditions (2.16) and (2.21) can be implemented. We illustrate this for case $N = 2$.

The following boundary conditions give dissipative boundary conditions to the above energy dissipation rate:

$$\begin{aligned} \frac{\partial \phi}{\partial t} = & - (M_s + \frac{\beta_1^2}{\alpha_1}) \tilde{\mu}_s + \frac{\beta_1}{\alpha_1} \tilde{\mu}, \quad \mathbf{x} \in \Gamma_1, \\ \alpha_1 \mathbf{n} \cdot \mathbf{M}_b^{(2)} \cdot \nabla \tilde{\mu} = & - \tilde{\mu} + \beta_1 \tilde{\mu}_s, \quad \mathbf{x} \in \Gamma_1, \\ \nabla_{\mathbf{n}} \phi_t = & - M_c \mu_c, \quad \mathbf{x} \in \Gamma_1, \\ \frac{\partial \phi}{\partial t} = & - M_s \tilde{\mu}_s - \frac{\beta_2}{\alpha_2} \tilde{\mu}, \quad \mathbf{x} \in \Gamma_2, \\ \alpha_2 \mathbf{n} \cdot \mathbf{M}_b^{(2)} \cdot \nabla \tilde{\mu} = & - \tilde{\mu} + \beta_2 \tilde{\mu}_s, \quad \mathbf{x} \in \Gamma_2, \\ \nabla_{\mathbf{n}} \phi_t = & - M_c \mu_c, \quad \mathbf{x} \in \Gamma_2. \end{aligned} \quad (2.37)$$

From (2.12), we have

$$\begin{aligned} \frac{dE}{dt} = & - \int_{\Omega} [\tilde{\mu} M_b^{(1)} \tilde{\mu} + \nabla \tilde{\mu} \cdot \mathbf{M}_b^{(2)} \cdot \nabla \tilde{\mu}] d\mathbf{x} + \int_{\Gamma_1} [\tilde{\mu}_s (\phi_t + \beta_1 \mathbf{n} \cdot \mathbf{M}_b^{(2)} \cdot \nabla \tilde{\mu})] ds \\ & - \frac{1}{\alpha_1} \int_{\Gamma_1} (\beta_1 \tilde{\mu}_s - \tilde{\mu})^2 ds - \int_{\Gamma_1} [\mu_c M_c \mu_c] ds + \int_{\Gamma_2} [\tilde{\mu}_s (\phi_t + \frac{\beta_2}{\alpha_2} \tilde{\mu})] ds \\ & - \frac{1}{\alpha_2} \int_{\Gamma_2} [\tilde{\mu}^2] ds - \int_{\Gamma_2} [\mu_c M_c \mu_c] ds. \end{aligned} \quad (2.38)$$

It is straightforward to generalize it to cases where $N > 2$. We note that the function space for the solution of the initial boundary value problems should be chosen such that weak derivatives exist in the bulk and on the surface. We will not elaborate on this in this paper.

2.5. Examples

We present a few free energy functionals for binary phase field models describing immiscible, miscible polymeric materials, molecular beam epitaxy (MBE) and crystal growth, respectively.

2.5.1. Polynomial double-well and Flory-Huggins mixing free energy for multiphase polymers

We consider a general free energy functional involving polynomial double well or Flory-Huggins bulk mixing energy and the conformational entropy in both the bulk and on the surface

$$\begin{aligned} E_b = & \int_{\Omega} [\frac{\rho}{2} \phi_t^2 + \frac{\gamma_1}{2} \nabla \phi \cdot \mathbf{D} \cdot \nabla \phi + \gamma_2 f(\phi)] d\mathbf{x}, \\ E_s = & \int_{\partial\Omega} [\frac{\rho_s}{2} \phi_t^2 + \frac{\zeta_1}{2} \nabla_s \phi \cdot \mathbf{D}_s \cdot \nabla_s \phi + \zeta_2 g(\phi)] ds, \end{aligned} \quad (2.39)$$

where ϕ is a phase variable vector, \mathbf{D} and \mathbf{D}_s are the positive semi-definite anisotropic coefficients of the conformational entropy in the bulk and surface [31, 57, 63], respectively, $\gamma_i, \zeta_i, i = 1, 2$ are parameters. The corresponding dynamic governing equations are given by setting $\mu_c = M_c = 0$ in (2.16) and (2.21).

2.5.2. Free energy for molecular beam epitaxy

A bulk and a surface free energy for molecular beam epitaxy (MBE) are similar to (2.39), but with different choices of energy densities f and g [38, 60]:

$$\begin{aligned} E_b &= \int_{\Omega} \left[\frac{\rho}{2} \phi_t^2 + \frac{\gamma_1}{2} \nabla \phi \cdot \mathbf{D} \cdot \nabla \phi + \gamma_2 f(\phi) \right] d\mathbf{x}, \\ E_s &= \int_{\partial\Omega} \left[\frac{\rho_s}{2} \phi_t^2 + \frac{\zeta_1}{2} \nabla_s \phi \cdot \mathbf{D}_s \cdot \nabla_s \phi + \zeta_2 g(\phi) \right] ds. \end{aligned} \quad (2.40)$$

There are two choices of $(\phi)f$ and $g(\phi)$ in MBE models, one is

$$f(\phi) = \frac{1}{4}(1 - |\nabla\phi|^2)^2, \mathbf{x} \in \Omega, \quad g(\phi) = \frac{1}{4}(1 - |\nabla\phi|^2)^2, \mathbf{x} \in \partial\Omega, \quad (2.41)$$

with slope selection and the other is

$$f(\phi) = -\frac{1}{2} \ln(1 + |\nabla\phi|^2), \mathbf{x} \in \Omega, \quad g(\phi) = -\frac{1}{2} \ln(1 + |\nabla\phi|^2), \mathbf{x} \in \partial\Omega, \quad (2.42)$$

without slope selection. Setting $\mu_c = M_c = M_b^{(2)} = 0$, we obtain the desired dynamic equations from (2.16) and (2.21).

2.5.3. Free energy for crystal growth models

A bulk free energy for the phase field crystal growth model is given by

$$E_b = \int_{\Omega} \left[\frac{\rho}{2} \phi_t^2 + \frac{\phi}{2} (-\epsilon + (\nabla^2 + 1)^2) \phi + \frac{\phi^4}{4} \right] d\mathbf{x}, \quad (2.43)$$

where ϕ represents an atomistic density field, which is the deviation of the density from the average density and is a conserved field variable, ϵ is a parameter related to the temperature, that is, higher ϵ corresponds to a lower temperature [11, 12].

Likewise, we propose the following for the surface energy

$$E_s = \int_{\partial\Omega} \left[\frac{\rho_s}{2} \phi_t^2 + \frac{1}{2} (\nabla_s^2 \phi)^2 - |\nabla_s \phi|^2 + g(\phi) \right] ds, \quad (2.44)$$

where $g(\phi)$ is a prescribed surface energy density. The corresponding governing equations, boundary conditions and energy dissipation rates are given by (2.16) and (2.21) with the free energy functionals substituted, respectively. We could also consider an anisotropic phase-field crystal model by using anisotropic conformational entropy in the bulk and the surface energy functional [37].

3. Nonlocal models and other extensions

We now consider phase field models with a nonlocal free energy [19, 25], where the free energy is given by

$$E_b = \int_{\Omega} \left[\int_{\Omega} \frac{1}{4} J(\|\mathbf{x} - \mathbf{y}\|) (\phi(\mathbf{x}, t) - \phi(\mathbf{y}, t))^2 d\mathbf{y} + f(\phi) \right] d\mathbf{x}, \quad (3.1)$$

where $J(\|\mathbf{x}\|)$ is the interaction kernel and f is the free energy density for the bulk. We assume the interaction between the bulk and the boundary has been built in the interaction kernel. This form of the free energy is perhaps more generic than the one that depends on spatial derivatives of the phase variable.

The chemical potential is calculated as follows

$$\mu = \int_{\Omega} J(\|\mathbf{x} - \mathbf{y}\|) (-\phi(\mathbf{y}, t)) d\mathbf{y} + f'(\phi) + a(\mathbf{x})\phi(\mathbf{x}, t), \quad (3.2)$$

where $a(\mathbf{x}) = \int_{\Omega} J(\|\mathbf{x} - \mathbf{y}\|) d\mathbf{y}$. Likewise, we consider the surface energy given by

$$E_s = \int_{\partial\Omega} \left[\int_{\partial\Omega} \frac{1}{4} K(\|\mathbf{x} - \mathbf{y}\|) (\phi(\mathbf{x}, t) - \phi(\mathbf{y}, t))^2 ds_{\mathbf{y}} + g(\phi) \right] ds_{\mathbf{x}}, \quad (3.3)$$

where g is the surface energy density. The surface chemical potential is calculated as follows

$$\begin{aligned} \mu_s &= \int_{\partial\Omega} K(\|\mathbf{x} - \mathbf{y}\|) (\phi(\mathbf{x}, t) - \phi(\mathbf{y}, t)) ds_{\mathbf{y}} + g'(\phi) \\ &= \int_{\partial\Omega} K(\|\mathbf{x} - \mathbf{y}\|) (-\phi(\mathbf{y}, t)) ds_{\mathbf{y}} + g'(\phi) + a_S(\mathbf{x}) \phi(\mathbf{x}, t), \end{aligned} \quad (3.4)$$

where $a_S(\mathbf{x}) = \int_{\partial\Omega} K(\|\mathbf{x} - \mathbf{y}\|) ds_{\mathbf{y}}$. The total free energy, including the inertia effect, is then given by

$$E = E_b + E_s + \int_{\Omega} \frac{\rho}{2} (\phi_t)^2 d\mathbf{x} + \int_{\partial\Omega} \frac{\rho_s}{2} (\phi_t)^2 ds. \quad (3.5)$$

We calculate the time rate of change of the free energy

$$\frac{d}{dt} E = \int_{\Omega} \tilde{\mu} \phi_t d\mathbf{x} + \int_{\partial\Omega} \tilde{\mu}_s \phi_t ds_{\mathbf{x}}. \quad (3.6)$$

We apply the Onsager principle to the bulk term to arrive at

$$\phi_t = -M_b \tilde{\mu}, \quad \mathbf{x} \in \Omega, \quad (3.7)$$

where M_b is the mobility operator. For $M_b = M_b^{(1)} - \nabla \cdot \mathbf{M}_b^{(2)} \cdot \nabla$,

$$\begin{aligned} \frac{d}{dt} E &= - \int_{\Omega} [\tilde{\mu} M_b^{(1)} \tilde{\mu} + \nabla \tilde{\mu} \cdot \mathbf{M}_b^{(2)} \cdot \nabla \tilde{\mu}] d\mathbf{x} + \int_{\partial\Omega} [\tilde{\mu}_s \phi_t + \tilde{\mu} \mathbf{n} \cdot \mathbf{M}_b^{(2)} \cdot \nabla \tilde{\mu}] dS_{\mathbf{x}} \\ &= - \int_{\Omega} [\tilde{\mu} M_b^{(1)} \tilde{\mu} + \nabla \tilde{\mu} \cdot \mathbf{M}_b^{(2)} \cdot \nabla \tilde{\mu}] d\mathbf{x} + \int_{\partial\Omega} [\tilde{\mu}_s \phi_t + \tilde{\mu} f_m] ds. \end{aligned} \quad (3.8)$$

We propose boundary condition as follows

$$\begin{pmatrix} \phi_t \\ f_m \end{pmatrix} = -M_{2 \times 2} \cdot \begin{pmatrix} \tilde{\mu}_s \\ \tilde{\mu} \end{pmatrix}, \quad \mathbf{x} \in \partial\Omega, \quad (3.9)$$

where $M_{2 \times 2} \geq 0$ is the boundary mobility operator.

The energy dissipation rate is given by

$$\frac{d}{dt} E = - \int_{\Omega} [\tilde{\mu} M_b^{(1)} \tilde{\mu} + \nabla \tilde{\mu} \cdot \mathbf{M}_b^{(2)} \cdot \nabla \tilde{\mu}] d\mathbf{x} - \int_{\partial\Omega} [(\tilde{\mu}_s, \tilde{\mu}) \cdot M_{2 \times 2} \cdot (\tilde{\mu}_s, \tilde{\mu})^T] ds. \quad (3.10)$$

By specifying $M_{2 \times 2}$ as the 2×2 upper left sub-matrix in $M_{3 \times 3}$ in the previous section, we arrive at two types of dynamic boundary conditions analogous to the above mentioned, which we will not repeat them here. We note that the authors derived a nonlocal model with the first type of dynamic boundary conditions and proved the weak and strong well-posedness of the system recently in [36] although they used two distinct phase field variables for the bulk and surface respectively.

The dynamic boundary conditions for the nonlocal model are similar to the ones with weakly nonlinear interactions through high order derivatives except that the chemical potential and the time rate of change of the phase field variable at the boundary do not have the explicit dependence on the bulk chemical potential. The explicit connection between the bulk

and the surface is in fact established through the nonlocal kernel in the free energy in the bulk effectively.

In the previous section, we present the results for a free energy with up to the second order spatial derivatives. This can be readily extended to include more general free energy functionals. It requires one to consider physically i) what would be the appropriate boundary conditions when the variation of the free energy is carried; ii) when the mobility operator includes high order spatial differential operators, how to deal with the boundary terms generated while applying integrations by parts in the context of thermodynamical consistency. The method presented here should be able to guide the generalization to those cases straightforwardly.

4. Numerical results

In this section, we use the crystal growth model alluded to earlier, as an example, to illustrate the effect of dynamic boundary conditions to the solution in the bulk numerically. We adopt the energy quadratization (EQ) and finite difference method to discretize the governing equation of the phase field crystal growth model [28, 29]. We assume the dimensionless bulk free energy and surface energy in a fixed rectangle domain are given respectively by

$$\begin{aligned} E_b &= \int_{\Omega} \left[\frac{|\nabla^2 \phi|^2}{2} - |\nabla \phi|^2 + \frac{1-\epsilon}{2} \phi^2 + \frac{\phi^4}{4} \right] d\mathbf{x}, \\ E_s &= \int_{\partial\Omega} \left[\frac{|\nabla_s^2 \phi|^2}{2} - |\nabla_s \phi|^2 + \frac{1-\epsilon_s}{2} \phi^2 + \frac{\phi^4}{4} \right] ds, \end{aligned} \quad (4.1)$$

where ϵ, ϵ_s are positive constant parameters. The corresponding chemical potentials in the bulk and on the boundary are calculated as follows

$$\begin{aligned} \mu &= \nabla^4 \phi + 2\nabla^2 \phi + (1-\epsilon)\phi + \phi^3, \quad \mu_c = \nabla \nabla \phi : \mathbf{nn}, \\ \mu_s &= \nabla_s^4 \phi + 2\nabla_s^2 \phi + (1-\epsilon_s)\phi + \phi^3 - \nabla^3 \phi \cdot \mathbf{n} - 2\nabla \phi \cdot \mathbf{n} - \nabla_s \mathbf{n} : \nabla \nabla \phi. \end{aligned} \quad (4.2)$$

We present some numerical examples of the crystal growth model with dynamic boundary conditions on a part of the boundary. We use a 2D computational domain, in which the four sides are labeled as $\Gamma_1, \Gamma_2, \Gamma_3$ and Γ_4 , respectively. Dynamics in the bulk is governed by

$$\frac{\partial \phi}{\partial t} = M_b^{(2)} \nabla^2 \mu, \quad (4.3)$$

where $M_b^{(2)}$ is a positive constant, while dynamic boundary conditions on each boundary are given respectively by

$$\begin{aligned} \frac{\partial \phi}{\partial t} &= -(-M_s^{(2)} \nabla_s^2 + \frac{\beta_1^2}{\alpha_1}) \mu_s + \frac{\beta_1}{\alpha_1} \mu, \quad \alpha_1 M_b^{(2)} \mathbf{n} \cdot \nabla \mu = -\mu + \beta_1 \mu_s, \quad \mathbf{x} \in \Gamma_1 \\ \nabla_{\mathbf{n}} \phi_t &= M_c^{(2)} \nabla^2 \mu_c, \quad \mathbf{x} \in \Gamma_1, \quad \mathbf{n} \cdot \nabla \phi = \mathbf{n} \cdot \nabla^3 \phi = \mathbf{n} \cdot \nabla \mu = 0, \quad \mathbf{x} \in \Gamma_2, \Gamma_3, \Gamma_4. \end{aligned} \quad (4.4)$$

Namely, we allow dynamic boundary conditions on one side of the boundary and static boundary conditions on the rest.

We use the energy quadratization technique together with the Crank-Nicolson method in time, and the second order finite difference method on staggered grids in space to derive a thermodynamically consistent numerical algorithm by introducing two intermediate scalar variables in the bulk and on the surface, respectively. The numerical algorithm guarantees that the total energy dissipates in time and space [30]. Simulations of the crystal growth model with static, homogeneous Neumann boundary conditions uniformly along the boundary, corresponding to the case of a zero surface energy, can be found in [29].

In all simulations, solid crystallites with Hexagonal ordering in 2D is initially placed in the centre of the computational domain, which is assigned an average density $\bar{\phi}$. The initial condition is given by

$$\phi_0(\mathbf{r}) = \bar{\phi} + \mathbf{w}(\mathbf{r})(\mathbf{A}\phi_s(\mathbf{r})), \quad (4.5)$$

where

$$w(\mathbf{r}) = \begin{cases} (1 - (\frac{|\mathbf{r}-\mathbf{r}_0|}{\mathbf{d}_0})^2)^2 & \text{if } \frac{|\mathbf{r}-\mathbf{r}_0|}{\mathbf{d}_0} \leq 1, \\ 0 & \text{otherwise,} \end{cases} \quad (4.6)$$

$$\phi_s(\mathbf{r}) = \cos(\frac{q}{\sqrt{3}}y) \cos(qx) - \frac{1}{2} \cos(\frac{2q}{\sqrt{3}}y), \quad (4.7)$$

$\mathbf{r} = (x, y)$, \mathbf{r}_0 is the center coordinate of the domain, and \mathbf{d}_0 is $\frac{1}{6}$ of the domain length in the x-direction. The domain is given by $\Omega = [0, \frac{2\pi}{q}a] \times [0, \frac{\sqrt{3}\pi}{q}b]$, $a = 10$ and $b = 12$. The other parameter values are $\varepsilon = 0.325$, $\bar{\phi} = \frac{\sqrt{\varepsilon}}{2}$, $A = \frac{4}{5}(\bar{\phi} + \frac{\sqrt{15\varepsilon - 36\bar{\phi}^2}}{3})$ and $q = \frac{\sqrt{3}}{2}$. For the initial condition on the surface and the surface energy at the boundary, we set $\epsilon_s = \epsilon$ and $\phi = A\phi_s$ on Γ_1 as the first initial condition at the surface. We move the initial condition to the right by $6h_x$ as the second initial condition of ϕ on the boundary to check the potential grain boundary effects induced by the surface energy, where h_x is the spatial step size. For simplicity, we call these two initial conditions on the surface as ordered and shifted initial condition on the surface, respectively. Besides these, we set $M_b^{(2)} = M_s^{(2)} = 1$ and $M_c^{(2)} = 0$ in the following simulations.

In the following, we investigate the effect of the surface energy on the bulk structure by varying two parameters α_1, β_1 . At first, the ordered and shifted initial conditions on the surface are depicted in Figure 4.1-(a,d), respectively. Figure 4.1-(a-c) show that the crystal grows from the bulk and the surface simultaneously with the ordered initial condition without a grain boundary effect. Figure 4.1-(d-f) show the grain boundary effect induced by the shifted initial condition on the surface in the highlighted region. This simulation demonstrates that a dynamic boundary condition can significantly affect crystal growth in the bulk.

We then check the roles of α_1, β_1 by benchmarking against the result in Figure 4.1-(a-c). In Figure 4.2, a large α_1 suppresses the roles that the surface energy and bulk energy play in inducing the across boundary mass flux at the boundary and forces a nearly homogeneous Neumann boundary condition asymptotically for $\tilde{\mu}$. As the result, the surface can have very little impact on the bulk structure as shown in (a) to (c). For a small α_1 , on the other hand, the difference between the surface energy and bulk energy is amplified at the boundary to lead to a large across boundary mass flux. As the result, the crystal growth at the boundary is significantly accelerated as shown in Figure 4.2-(d) to (f).

β_1 is also varied while α_1 is fixed to show the effect of the surface energy on the bulk pattern in Figure 4.3. If β_1 is large, it forces a near static boundary state with $\mu_s \approx 0$. That is the reason why the pattern in the bulk is similar to the one with the homogeneous Neumann boundary condition shown in Figure 4.2-(a-c). If β_1 is small, crystal growth near the surface tends to form solid crystallites with weak hexagonal ordering resembling a lamellar pattern shown in Figure 4.3-(d-f). This prevents the well-ordered crystal from growing into the boundary region. The time evolutions of total energy, bulk energy and surface energy in figure 4.4 show that the total free energy dissipation is guaranteed. However, the surface energy may increase due to the mass transfer at the boundary. The patterns in figure 4.2-(a-c) and 4.3-(a-c) are similar because their bulk energies are the same as in 4.4-(b), however, their surface free energies are different. The difference of surface energies between them are covered by the magnitude of

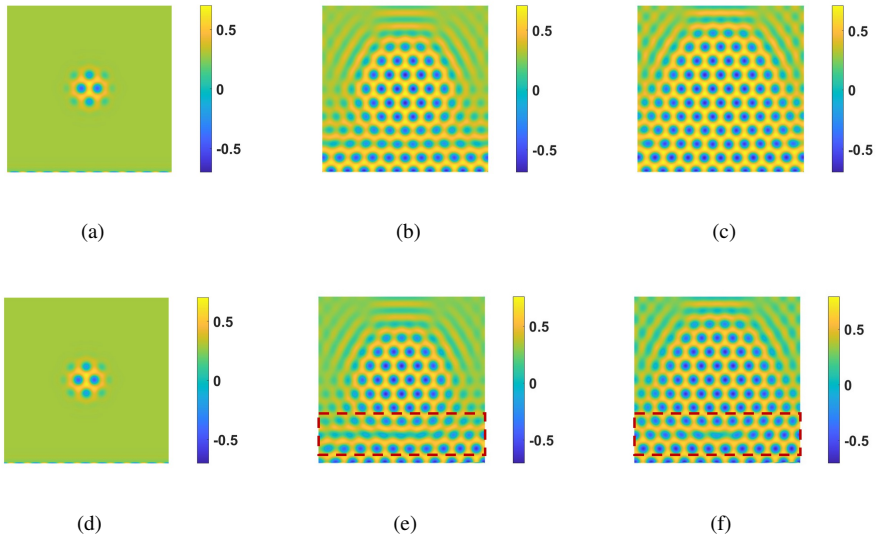


FIG. 4.1. *The ordered growth vs the grain boundary effect induced by a shifted initial boundary condition in (d)-(f). Snapshots of the numerical solution of ϕ are taken with 128×128 meshes in 2D space at $T=0, 32, 40$, respectively. Time step $\delta t = 1 \times 10^{-2}$ and $\alpha_1 = \beta_1 = 1$ are used in the simulations. (a)-(c): $\phi = A\phi_s$ is used at boundary Γ_1 ; (d)-(f): the shifted initial boundary condition is used in the simulation, where the grain boundary effect was shown in the highlighted region.*

the bulk energy. Figure 4.4 show numerically that both α_1 and β_1 control the magnitude of the energies.

In the example, we demonstrate that the surface energy and prescribed dynamic boundary conditions can indeed influence bulk dynamics in various ways depending on what surface physical effects are dominating. It paves the way for one to alter or even manipulate bulk dynamics by controlling the boundary condition especially when the bulk energy and surface energy become comparable in a small confined geometry.

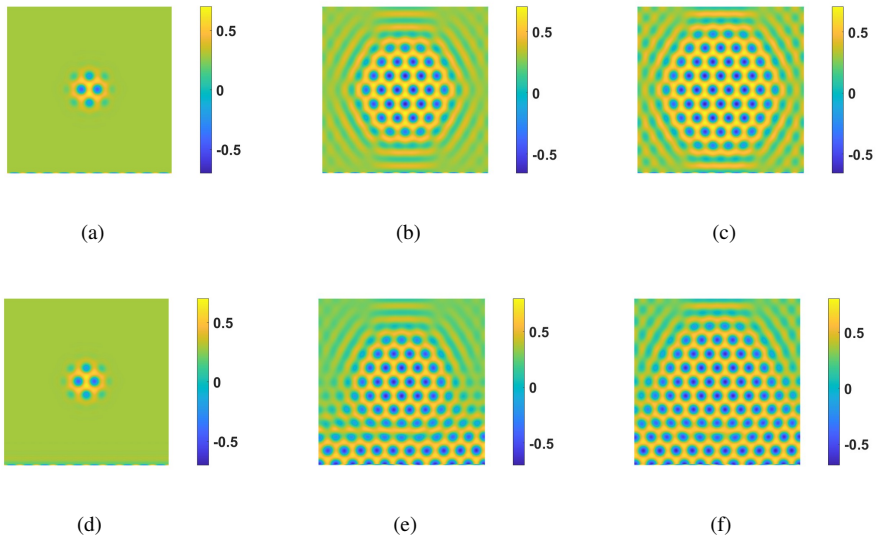


FIG. 4.2. The role of model parameter α_1 in the ordered growth. The snapshots of ϕ are taken with 128×128 space meshes at $T = 0, 32, 40$, respectively. Time step $\delta t = 1 \times 10^{-2}$ is used. (a)-(c): $\alpha_1 = 1 \times 10^3, \beta_1 = 1$; (d)-(f): $\alpha_1 = 5 \times 10^{-3}, \beta_1 = 1$. A large α_1 tends to annihilate the boundary effect to the bulk while a small α_1 promotes crystal growth near the boundary in addition to the growth in the middle and thereby facilitates the overall growth in the domain.

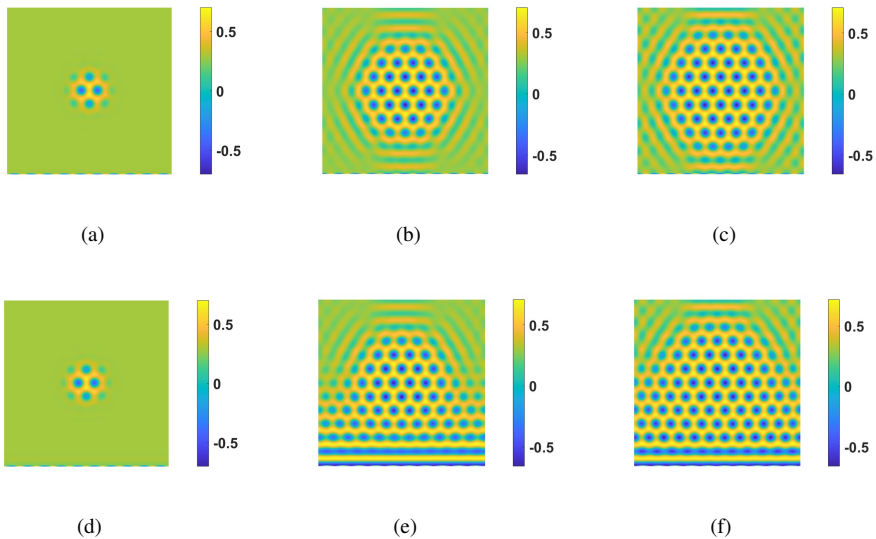


FIG. 4.3. The role of parameter β_1 in the ordered growth. Snapshots of ϕ are taken with 128×128 space meshes at $T = 0, 32, 40$, respectively. Time step is chosen as $\delta t = 1 \times 10^{-2}$. (a)-(c): $\alpha_1 = 1, \beta_1 = 10$; (d)-(f): $\alpha_1 = 1, \beta_1 = 1 \times 10^{-4}$. A large β_1 diminishes the effect of boundary dynamics while a small β_1 facilitates growth near the boundary in a different pattern.

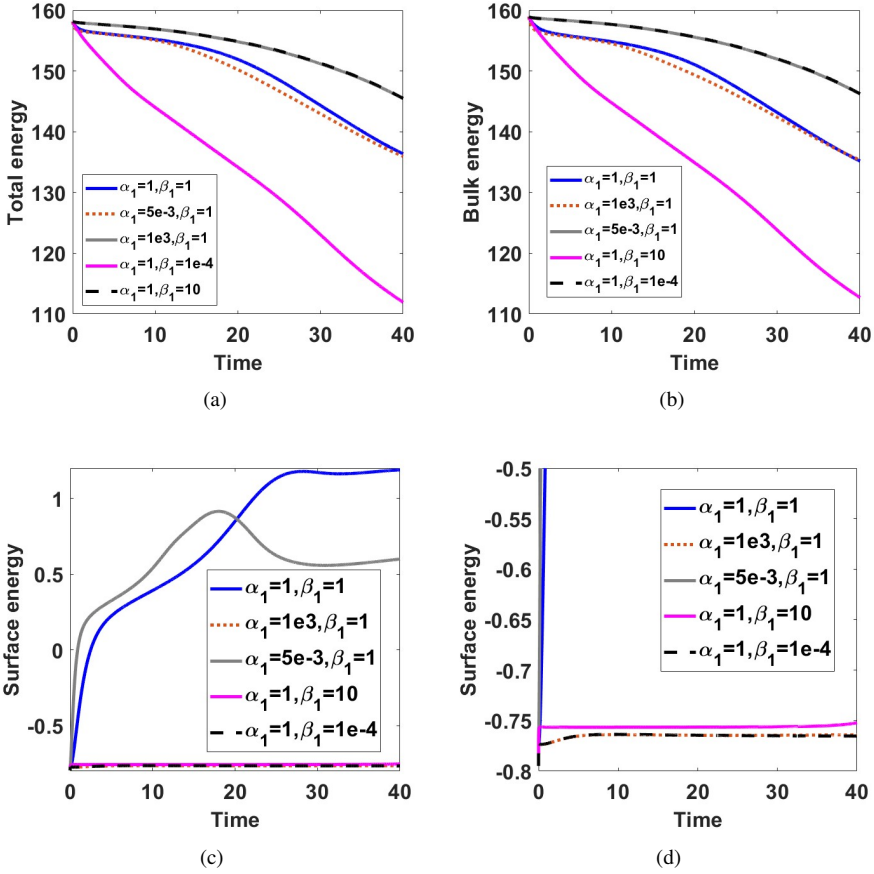


FIG. 4.4. Time evolutions of total energy, bulk energy and surface energy with different α_1, β_1 in (a-c). In (d), the range of surface energies are between $[-0.8, -0.5]$, which is a supplementary figure for (c). Though the surface energies for $\alpha_1 = 1 \times 10^3, \beta_1 = 1$ and $\alpha_1 = 1, \beta_1 = 1 \times 10^{-4}$ are almost same, their bulk free energies are different. The bulk free energies for $\alpha_1 = 5 \times 10^{-3}, \beta_1 = 1$ and $\alpha_1 = 1, \beta_1 = 1 \times 10^{-4}$ are also almost same, but their surface free energies are different. It reveals the magnitudes of the bulk and surface energies and the weights for chemical potentials or flux determine the patterns.

5. Conclusions

We have presented a hierarchical procedure for deriving thermodynamically consistent models together with consistent dynamic boundary conditions using the generalized Onsager principle in tandem. We illustrate it using the binary phase field model with up to second order spatial derivatives in the free energy functional. Extensions to models with more general free energy functionals, including the one with nonlocal interaction kernels, can be derived following an analogous procedure. We show that many existing binary phase field models with the dynamic/static boundary conditions are in fact special cases of the general model. We then show the effect of the surface energy and the dynamic boundary conditions on solutions in the bulk in crystal growth processes through numerical simulations. This study summarizes a thermodynamically consistent modeling protocol. It also paves the way for one to develop structural preserving, thermodynamically consistent numerical algorithms for the resulting models.

Acknowledgements. Xiaobo Jing’s research is partially supported by NSFC awards #11971051, #12147165 and NSAF-U1930402 to CSRC. Qi Wang’s research is partially supported by NSF awards OIA-1655740 and a GEAR award from SC EPSCoR/IDeA Program.

REFERENCES

- [1] Samuel M Allen and John W Cahn. A microscopic theory for antiphase boundary motion and its application to antiphase domain coarsening. *Acta metallurgica*, 27(6):1085–1095, 1979. 1, 1
- [2] Howard Brenner. *Interfacial transport processes and rheology*. Elsevier, 2013. 1
- [3] John W Cahn and John E Hilliard. Free energy of a nonuniform system. i. interfacial free energy. *The Journal of chemical physics*, 28(2):258–267, 1958. 1, 1
- [4] Cecilia Cavaterra, Maurizio Grasselli, and Hao Wu. Non-isothermal viscous cahn-hilliard equation with inertial term and dynamic boundary conditions. *Communications on Pure & Applied Analysis*, 13(5):1855, 2014. 1
- [5] Chun-Wei Chen, Chien-Tsung Hou, Cheng-Chang Li, Hung-Chang Jau, Chun-Ta Wang, Ching-Lang Hong, Duan-Yi Guo, Cheng-Yu Wang, Sheng-Ping Chiang, Timothy J Bunning, et al. Large three-dimensional photonic crystals based on monocrystalline liquid crystal blue phases. *Nature communications*, 8(1):1–8, 2017. 1
- [6] Long-Qing Chen. Phase-field models for microstructure evolution. *Annual review of materials research*, 32(1):113–140, 2002. 1
- [7] Laurence Cherfilis, Alain Miranville, and Sergey Zelik. The cahn-hilliard equation with logarithmic potentials. *Milan Journal of Mathematics*, 79(2):561–596, 2011. 1
- [8] Pierluigi Colli and Takeshi Fukao. Cahn–hilliard equation with dynamic boundary conditions and mass constraint on the boundary. *Journal of Mathematical Analysis and Applications*, 429(2):1190–1213, 2015. 1
- [9] Pierluigi Colli, Takeshi Fukao, and Kei Fong Lam. On a coupled bulk–surface allen–cahn system with an affine linear transmission condition and its approximation by a robin boundary condition. *Nonlinear Analysis*, 184:116–147, 2019. 1
- [10] Gerhard Dziuk and Charles M Elliott. Finite element methods for surface pdes. *Acta Numerica*, 22:289–396, 2013. 1, 1
- [11] Ken R Elder, Nikolas Provatas, Joel Berry, Peter Stefanovic, and Martin Grant. Phase-field crystal modeling and classical density functional theory of freezing. *Physical Review B*, 75(6):064107, 2007. 2.5.3
- [12] KR Elder and Martin Grant. Modeling elastic and plastic deformations in nonequilibrium processing using phase field crystals. *Physical Review E*, 70(5):051605, 2004. 2.5.3
- [13] KR Elder, Martin Grant, Nikolas Provatas, and JM Kosterlitz. Sharp interface limits of phase-field models. *Physical Review E*, 64(2):021604, 2001. 1
- [14] Hans Peter Fischer, Philipp Maass, and Wolfgang Dieterich. Novel surface modes in spinodal decomposition. *Physical review letters*, 79(5):893, 1997. 1
- [15] HP Fischer, J Reinhard, W Dieterich, J-F Gouyet, P Maass, A Majhofer, and D Reinel. Time-dependent density functional theory and the kinetics of lattice gas systems in contact with a wall. *The Journal of chemical physics*, 108(7):3028–3037, 1998. 1
- [16] Takeshi Fukao and Hao Wu. Separation property and convergence to equilibrium for the equation and dynamic boundary condition of cahn-hilliard type with singular potential. *arXiv preprint arXiv:1910.14177*, 2019. 1
- [17] Takeshi Fukao, Shuji Yoshikawa, and Saori Wada. Structure-preserving finite difference schemes for the cahn-

- hilliard equation with dynamic boundary conditions in the one-dimensional case. *Communications on Pure & Applied Analysis*, 16(5):1915, 2017. [1](#)
- [18] Ciprian G Gal. A cahn–hilliard model in bounded domains with permeable walls. *Mathematical methods in the applied sciences*, 29(17):2009–2036, 2006. [1](#), [2,3](#)
- [19] Ciprian G Gal. Doubly nonlocal cahn–hilliard equations. In *Annales de l’Institut Henri Poincaré C, Analyse non linéaire*, volume 35, pages 357–392. Elsevier, 2018. [3](#)
- [20] Ciprian G Gal and Hao Wu. Asymptotic behavior of a cahn–hilliard equation with wenzell boundary conditions and mass conservation. *Discrete & Continuous Dynamical Systems-A*, 22(4):1041, 2008. [1](#)
- [21] Peter Galenko and David Jou. Diffuse-interface model for rapid phase transformations in nonequilibrium systems. *Physical Review E*, 71(4):046125, 2005. [1](#)
- [22] PK Galenko and D Jou. Rapid solidification as non-ergodic phenomenon. *Physics Reports*, 818:1–70, 2019. [1](#)
- [23] Harald Garcke and Patrik Knopf. Weak solutions of the cahn–hilliard system with dynamic boundary conditions: A gradient flow approach. *SIAM Journal on Mathematical Analysis*, 52(1):340–369, 2020. [1](#)
- [24] Sergey Gavriluk and Henri Gouin. Dynamic boundary conditions for membranes whose surface energy depends on the mean and gaussian curvatures. *Mathematics and Mechanics of Complex Systems*, 7(2):131–157, 2019. [1](#)
- [25] Giambattista Giacomin and Joel L Lebowitz. Phase segregation dynamics in particle systems with long range interactions. i. macroscopic limits. *Journal of statistical Physics*, 87(1-2):37–61, 1997. [3](#)
- [26] Gisèle Ruiz Goldstein, Alain Miranville, and Giulio Schimperna. A cahn–hilliard model in a domain with non-permeable walls. *Physica D: Nonlinear Phenomena*, 240(8):754–766, 2011. [1](#), [2,3](#)
- [27] Alexander Grigoryan. *Heat kernel and analysis on manifolds*, volume 47. American Mathematical Soc., 2009. [1](#)
- [28] Xiaobo Jing, Jun Li, Xueping Zhao, and Qi Wang. Second order linear energy stable schemes for allen-cahn equations with nonlocal constraints. *Journal of Scientific Computing*, 80(1):500–537, 2019. [1](#), [4](#)
- [29] Xiaobo Jing and Qi Wang. Linear second order energy stable schemes for phase field crystal growth models with nonlocal constraints. *Computers & Mathematics with Applications*, 79(3):764–788, 2020. [1](#), [4](#), [4](#)
- [30] Xiaobo Jing and Qi Wang. Structure preserving algorithms for thermodynamically consistent partial differential equation with dynamical boundary conditions. *to be submitted*, 2022. [4](#)
- [31] Alain Karma and Wouter-Jan Rappel. Phase-field model of dendritic sidebranching with thermal noise. *Physical review E*, 60(4):3614, 1999. [2.5](#), [1](#)
- [32] Rainer Kenzler, Frank Eurich, Philipp Maass, Bernd Rinn, Johannes Schropp, Erich Bohl, and Wolfgang Dieterich. Phase separation in confined geometries: Solving the cahn–hilliard equation with generic boundary conditions. *Computer Physics Communications*, 133(2-3):139–157, 2001. [1](#)
- [33] Junseok Kim. Phase-field models for multi-component fluid flows. *Communications in Computational Physics*, 12(3):613–661, 2012. [1](#)
- [34] Patrik Knopf and Kei Fong Lam. Convergence of a robin boundary approximation for a cahn–hilliard system with dynamic boundary conditions. *arXiv preprint arXiv:1908.06124*, 2019. [1](#)
- [35] Patrik Knopf, Kei Fong Lam, Chun Liu, and Stefan Metzger. Phase-field dynamics with transfer of materials: The cahn–hillard equation with reaction rate dependent dynamic boundary conditions. *arXiv preprint arXiv:2003.12983*, 2020. [1](#), [2,3](#)
- [36] Patrik Knopf and Andrea Signori. On the nonlocal cahn–hilliard equation with nonlocal dynamic boundary condition and boundary penalization. *Journal of Differential Equations*, 280:236–291, 2021. [1](#), [2,3](#), [3](#)
- [37] Julia Kundin and Muhammad Ajmal Choudhary. Application of the anisotropic phase-field crystal model to investigate the lattice systems of different anisotropic parameters and orientations. *Modelling and Simulation in Materials Science and Engineering*, 25(5):055004, 2017. [2.5](#), [3](#)
- [38] Bo Li and Jian-Guo Liu. Thin film epitaxy with or without slope selection. *European Journal of Applied Mathematics*, 14(6):713–743, 2003. [2.5](#), [2](#)
- [39] Jun Li, Jia Zhao, and Qi Wang. Energy and entropy preserving numerical approximations of thermodynamically consistent crystal growth models. *Journal of Computational Physics*, 382:202–220, 2019. [1](#)
- [40] Chun Liu and Hao Wu. An energetic variational approach for the cahn–hilliard equation with dynamic boundary condition: model derivation and mathematical analysis. *Archive for Rational Mechanics and Analysis*, 233(1):167–247, 2019. [1](#), [2,3](#)
- [41] José A Martínez-González, Ye Zhou, Mohammad Rahimi, Emre Bukusoglu, Nicholas L Abbott, and Juan J de Pablo. Blue-phase liquid crystal droplets. *Proceedings of the National Academy of Sciences*, 112(43):13195–13200, 2015. [1](#)
- [42] Britta Nestler and Abhik Choudhury. Phase-field modeling of multi-component systems. *Current opinion in solid state and Materials Science*, 15(3):93–105, 2011. [1](#)
- [43] Makoto Okumura and Daisuke Furihata. A structure-preserving scheme for the allen–cahn equation with a dynamic boundary condition. *Discrete & Continuous Dynamical Systems-A*, 40(8):4927, 2020. [1](#)
- [44] Lars Onsager. Reciprocal relations in irreversible processes. i. *Physical review*, 37(4):405, 1931. [1](#), [2,1](#)
- [45] Lars Onsager. Reciprocal relations in irreversible processes. ii. *Physical review*, 38(12):2265, 1931. [1](#), [2,1](#)
- [46] Lars Onsager and Stefan Machlup. Fluctuations and irreversible processes. *Physical Review*, 91(6):1505, 1953.

2.1

- [47] Nikolas Provatas and Ken Elder. *Phase-field methods in materials science and engineering*. John Wiley & Sons, 2011. [1](#)
- [48] MD Asiqur Rahman, Suhana Mohd Said, and S Balamurugan. Blue phase liquid crystal: strategies for phase stabilization and device development. *Science and technology of advanced materials*, 16(3):033501, 2015. [1](#)
- [49] Yevgeny Rakita, Igor Lubomirsky, and David Cahen. When defects become dynamic: halide perovskites: a new window on materials? *Materials Horizons*, 6(7):1297–1305, 2019. [1](#)
- [50] Piotr Rybka and Karl-Heinz Hoffmann. Convergence of solutions to cahn-hilliard equation. *Communications in partial differential equations*, 24(5-6):1055–1077, 1999. [1](#)
- [51] A Salhoumi and PK Galenko. Gibbs–thomson condition for the rapidly moving interface in a binary system. *Physica A: Statistical Mechanics and its Applications*, 447:161–171, 2016. [1](#)
- [52] Irina Singer-Loginova and HM Singer. The phase field technique for modeling multiphase materials. *Reports on progress in physics*, 71(10):106501, 2008. [1](#)
- [53] Ingo Steinbach. Phase-field models in materials science. *Modelling and simulation in materials science and engineering*, 17(7):073001, 2009. [1](#)
- [54] Ingo Steinbach, Franco Pezzolla, Britta Nestler, Markus Seeßelberg, Robert Prieler, Georg J Schmitz, and Joao LL Rezende. A phase field concept for multiphase systems. *Physica D: Nonlinear Phenomena*, 94(3):135–147, 1996. [1](#)
- [55] Shouwen Sun, Jun Li, Jia Zhao, and Qi Wang. Structure-preserving numerical approximations to a non-isothermal hydrodynamic model of binary fluid flows. *Journal of Scientific Computing*, 83:50, 2020. [1](#)
- [56] Qi Wang. Generalized onsager principle and its application. In Xiang you Liu, editor, *Frontiers and Progress of Current Soft Matter Research*. Springer Nature, 2020. [1](#), [2.1](#)
- [57] James A Warren and William J Boettinger. Prediction of dendritic growth and microsegregation patterns in a binary alloy using the phase-field method. *Acta Metallurgica et Materialia*, 43(2):689–703, 1995. [2.5.1](#)
- [58] Hao Wu. A review on the cahn-hilliard equation: Classical results and recent advances in dynamic boundary conditions. *arXiv preprint arXiv:2112.13812*, 2021. [1](#)
- [59] Xiangjun Xing. Topology and geometry of smectic order on compact curved substrates. *Journal of Statistical Physics*, 134(3):487–536, 2009. [1](#)
- [60] Xiaofeng Yang, Jia Zhao, Qi Wang, and Jie Shen. Numerical approximations for a three-component cahn–hilliard phase-field model based on the invariant energy quadratization method. *Mathematical Models and Methods in Applied Sciences*, 27(11):1993–2030, 2017. [2.5.2](#)
- [61] Xiaogang Yang, Jun Li, M Gregory Forest, and Qi Wang. Hydrodynamic theories for flows of active liquid crystals and the generalized onsager principle. *Entropy*, 18(6):202, 2016. [1](#), [2.1](#)
- [62] Gil Ho Yoon. Topology optimization for nonlinear dynamic problem with multiple materials and material-dependent boundary condition. *Finite elements in analysis and design*, 47(7):753–763, 2011. [1](#)
- [63] Jia Zhao, Qi Wang, and Xiaofeng Yang. Numerical approximations for a phase field dendritic crystal growth model based on the invariant energy quadratization approach. *International Journal for Numerical Methods in Engineering*, 110(3):279–300, 2017. [2.5.1](#)
- [64] Jia Zhao, Xiaofeng Yang, Yuezheng Gong, Xueping Zhao, Xiaogang Yang, Jun Li, and Qi Wang. A general strategy for numerical approximations of non-equilibrium models-part i: thermodynamical systems. *Int. J. Numer. Anal. Model*, 15(6):884–918, 2018. [1](#)
- [65] Xueping Zhao, Tiezheng Qian, and Qi Wang. Thermodynamically consistent hydrodynamic models of multi-component fluid flows. *arXiv preprint arXiv:1809.05494*, 2018. [1](#)